Diagonalization of the Hamiltonian for finite-sized dispersive media: Canonical quantization with numerical mode decomposition

Dong-Yeop Na [1], Jie Zhu [1], and Weng C. Chew [1,2,*]

[1] *School of Electrical and Computer Engineering, Purdue University, West Lafayette Indiana, 47907, USA*

[2] *Purdue Quantum Science Engineering Institute, Purdue University, West Lafayette Indiana, 47907, USA*

(Received 10 October 2020; revised 27 January 2021; accepted 28 April 2021; published 10 June 2021)

We present a math-physics modeling approach called *canonical quantization with numerical mode decomposition* for capturing the physics of how incoming photons interact with finite-sized dispersive media, which is not describable by the previous Fano-diagonalization methods. The main procedure is to (1) study a system where electromagnetic fields are coupled to nonuniformly distributed Lorentz oscillators in Hamiltonian mechanics, (2) derive a generalized Hermitian eigenvalue problem for conjugate pairs in coordinate space, (3) apply computational electromagnetics methods to find a countably finite set of time-harmonic eigenmodes that diagonalizes the Hamiltonian, and (4) perform the subsequent canonical quantization with mode decomposition. Moreover, we provide several numerical simulations that capture the physics of full quantum effects, impossible by classical Maxwell's equations, such as nonlocal dispersion cancellation of an entangled photon pair and the Hong-Ou-Mandel effect in a dispersive beam splitter.

DOI: 10.1103/PhysRevA.103.063707

I. INTRODUCTION

A. Main contribution

We present a math-physics modeling approach, *canonical quantization with numerical mode decomposition* (CQ-NMD), suited for studying how incoming (entangled) photons interact with finite-sized dispersive media (see Fig. 1) which are not simply described by the previous Fano-diagonalization methods. To do this, we (1) study a system where electromagnetic (EM) fields are coupled to nonuniformly distributed Lorentz oscillators in Hamiltonian mechanics, (2) derive a generalized Hermitian eigenvalue problem (GH-EVP) for conjugate pairs in the coordinate space, (3) apply computational electromagnetics (CEM) methods to find a countably finite set of time-harmonic eigenmodes which diagonalize the Hamiltonian, and (4) perform the subsequent canonical quantization with mode decomposition. We consider two applications of this modeling for fully quantum effects including the Hong-Ou-Mandel (HOM) effects in a dispersive beam splitter and nonlocal dispersion cancellation (NLDC) for an energy-time entangled photon pair, showing that such CEM-driven quantum electromagnetics-optics (QEM-QO) research has great promise. In this way, nonlocal dispersion cancellation can be modeled by a numerical method that can be applied to a geometry of arbitrary complexity.

Pioneering theoretical works [1,2] have shown canonical quantization schemes for dispersionless, lossless, and inhomogeneous dielectric media. In essence, the underlying principle is the same as that of free fields. Furthermore, it is shown in our recent study [3] that solving for the eigenmodes can be numerically performed by exploiting CEM methods. Such CEM-driven QEM-QO simulations have a great potential for effectively dealing with practical QEM-QO applications involving arbitrary geometric complexity, such as in quantum imaging, sensing, and radar.

According to Ref. [4], the free-field contribution should be added to the previous Fano-diagonalization-based quantization scheme so that one can accurately model finite-sized media illuminated by incoming photons from free space. The complete description was recently proposed by Ref. [5] in momentum (or spectral) space. We show that our formulation is mathematically equivalent to theirs although our formulation is in coordinate space with the use of CEM methods. Thus, the proposed approach can tackle arbitrary geometrical complexity present in finite-sized dispersive media. Also, our work and derivations are based on sound mathematical logic and validated with numerical studies. Then we use our math-physics model to reproduce the "weird" physical phenomena that have been reported in the literature.

Our main contributions are threefold:

(i) We derive a GH-EVP for EM fields coupled to nonuniformly distributed Lorentz oscillators, which model finite-sized dispersive media, directly in coordinate space.

(ii) We exploit CEM methods to solve the GH-EVP with arbitrary geometric complexity to obtain a countably finite set of time-harmonic eigenmodes that diagonalizes the Hamiltonian; hence, the subsequent quantization becomes easier.

(iii) Our approach is suitable for studying interactions between incoming (entangled) photons from the free space with arbitrary finite-sized dispersive media, such as quantum plasmonic devices or quantum low-loss optical components. These cannot be modeled by the previous Fano-diagonalization methods.

Also, from our model, we can see clearly the dressing of the modes of the system due to coupling between free-field modes and the material modes. Moreover, we can clearly see from the math that when the material medium is removed or

*wcchew@purdue.edu

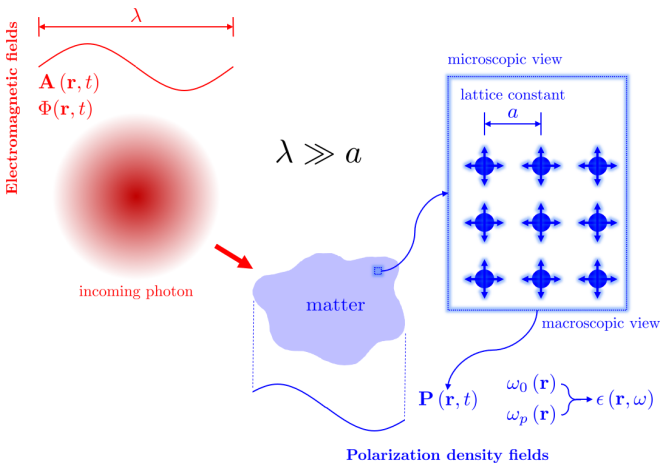

FIG. 1. Two-dimensional illustration of a problem geometry where electromagnetic fields are coupled to lossless Lorentz oscillators forming polarization density fields inside a macroscopic dispersive and inhomogeneous dielectric medium.

shrunk to zero, we retrieve the free-field modes and vice versa. This is not easy to observe when the Fano diagonalization approach is used.

Although we present the GH-EVP for the generalized Lorenz gauge, all numerical simulations are performed with the Coulomb gauge. Thus it is equivalent to the Lorenz gauge with zero scalar potential, to reduce the redundancy of the longitudinal component of the vector potential.

We use the Bloch-periodic boundary conditions (B-PBCs) on the GH-EVP to simulate an infinite-region problem. When the period tends to infinity, we retrieve the open infinite-region case. Hence, the GH-EVP is exactly Hermitian. The B-PBC is the generalized version of conventional PBC, allowing one to extract eigenmodes in the traveling-wave form in the presence of arbitrary, lossless, inhomogeneous media. As a result, the subsequent quantization procedure becomes mathematically homomorphic to that of free space. Note that, despite working with lossless media, the Kramers-Kronig relation is still satisfied [6].

B. Reviews of previous macroscopic quantum electrodynamics work

The quantum nature of EM fields is basically captured by solving the quantum Maxwell's equations (QMEs) [7–10] together with solving the quantum state equation. In the QMEs, the classical Maxwell field and source variables are elevated to infinite-dimensional quantum *operators*, expressible by

$$\begin{aligned}
\nabla \times \hat{\mathbf{E}}(\mathbf{r},t) &= -\frac{\partial \hat{\mathbf{B}}(\mathbf{r},t)}{\partial t},\\
\nabla \times \hat{\mathbf{H}}(\mathbf{r},t) &= \hat{\mathbf{J}}(\mathbf{r},t) + \frac{\partial \hat{\mathbf{D}}(\mathbf{r},t)}{\partial t},\\
\nabla \cdot \hat{\mathbf{D}}(\mathbf{r},t) &= \hat{\rho}(\mathbf{r},t),\\
\nabla \cdot \hat{\mathbf{B}}(\mathbf{r},t) &= 0,
\end{aligned} \tag{1}$$

The quantum state equations (QSEs) take the form of

$$\hat{H}\,|\psi\rangle = i\hbar\frac{\partial}{\partial t}\,|\psi\rangle\,, \tag{2}$$

where $\hat{H}$ and $|\psi\rangle$ denote a Hamiltonian operator and quantum state, respectively. This equation is often called Schrödinger equation, but when the Hamiltonian is replaced by the Dirac Hamiltonian, then it is often called the Dirac equation [11]. To avoid the confusion, we shall call it the quantum state equation, since we are using an EM Hamiltonian which is very different from Schrödinger's original Hamiltonian.

With the quantum state known, one can evaluate the expectation value or variance of observables. Note that the above QMEs are rigorously derived in the Heisenberg picture, in coordinate space, for inhomogeneous and anisotropic media when impressed sources are present [10]. The space and time dependence of field operators obeys QMEs, similar to the classical Maxwellian variables. On the other hand, the weird properties such as "superposition" and "entanglement" can be modeled by solving the QSE. Having no classical analog, such properties are the main reason for the weird performance beyond the classical limit.

In place of the atomistic description, the macroscopic theory on quantum electrodynamics (QED), proposed by Jauch and Watson [12], is more practical to analyze large-scale quantum technologies. This framework is valid as long as the wavelength of photons is much larger than a lattice constant [13,14]. In this, the EM characteristics of matter (composed of a large number of atoms) are embodied in a phenomenological medium described by the effective permittivity and permeability, as done in the classical Maxwell theory. Thus, it can reduce significantly the needed degrees of freedom (DoFs) for modeling. This approach has been successfully applied to study various quantum-related applications, for instance, quantum metamaterials [15], Casimir forces [16], spontaneous emission in photonic structures [17], and quantum plasmonics [18], just to name a few.

Recently, Jauslin's group has shown that the previous Fano-diagonalization method is incomplete when it comes to studying finite-sized dispersive and dissipative media [4]. Specifically, in the vanishing limit of finite-sized media, the previous Fano-diagonalization approach, which only includes the medium-assisted field operators, cannot recover the free-field operator due to the absence of the free-field contribution. Hence, the Fano-diagonalization approach violates a simple sanity check. The complete quantization formulation was proposed in Ref. [5] in momentum space.

But analytic solutions of time-harmonic eigenmodes are often not available. More importantly, the corresponding Helmholtz wave equation for vector potentials,

$$\nabla \times \frac{1}{\mu_0}\nabla \times \tilde{\mathbf{A}}(\mathbf{r}) - \underbrace{\omega^2\epsilon(\mathbf{r},\omega)}_{\text{eigenvalue}}\tilde{\mathbf{A}}(\mathbf{r}) = 0, \tag{3}$$

cannot be converted to a simple explicit eigenvalue problem (EVP) since the eigenvalue ω is implicit. As such, the two fundamental properties essential for canonical quantizations of systems does not hold in a strict sense: (1) completeness of eigenmodes and (2) realness of eigenfrequency. Nevertheless, such implicit EVP have been solved by some *ad hoc* fashions

in the past, such as the finite-difference time-domain (FDTD) method, iterative eigenvalue algorithms, or the cutting surface method [19]. In contrast, we formulate this as an explicit eigenvalue problem here.

II. DIAGONALIZATION OF CLASSICAL HAMILTONIAN VIA TIME-HARMONIC EIGENMODES

A. Description in Hamiltonian mechanics

Consider EM fields coupled to a cluster of lossless Lorentz oscillators in the three-dimensional free space V, as illustrated in Fig. 1. Lorentz (or medium) oscillators can be nonuniformly distributed over V, modeling an arbitrary lossless, isotropic, dispersive, and inhomogeneous dielectric medium.

Fundamental dynamical variables are vector and scalar potentials and polarization density field, denoted by $\mathbf{A}$, Φ, and $\mathbf{P}$, respectively. Suggested in Ref. [20], we define the conjugate variables $\mathbf{A}$, Φ, and $\mathbf{P}$ as

$$\mathbf{\Pi}_{AP} \triangleq \epsilon_0 \frac{\partial \mathbf{A}}{\partial t} - \mathbf{P}, \quad \Pi_\Phi \triangleq \chi_0 \frac{\partial \Phi}{\partial t}, \quad \mathbf{\Pi}_P \triangleq \frac{\beta(\mathbf{r})}{\epsilon_0} \frac{\partial \mathbf{P}}{\partial t}. \tag{4}$$

The corresponding Hamiltonian is then given by

$$\begin{aligned} H = \int_V d\mathbf{r} \mathcal{H}(\mathbf{r}, t) = \frac{1}{2} \int_V d\mathbf{r} \Big(& \frac{1}{\epsilon_0} |\mathbf{\Pi}_{AP}|^2 + \frac{1}{\mu_0} |\nabla \times \mathbf{A}|^2 \\ & + \frac{1}{\chi_0} (\nabla \cdot \epsilon_0 \mathbf{A})^2 - \epsilon_0 |\nabla \Phi|^2 - \frac{1}{\chi_0} \Pi_\Phi^2 + \frac{\epsilon_0}{\beta(\mathbf{r})} |\mathbf{\Pi}_P|^2 \\ & + \frac{f(\mathbf{r}) + 1}{\epsilon_0} |\mathbf{P}|^2 + \frac{2}{\epsilon_0} \mathbf{\Pi}_{AP} \cdot \mathbf{P} + 2\mathbf{P} \cdot \nabla \Phi \Big), \end{aligned} \tag{5}$$

where $f(\mathbf{r}) = \omega_0^2(\mathbf{r})/\omega_p^2(\mathbf{r})$ and $\beta(\mathbf{r}) = 1/\omega_p^2(\mathbf{r})$. Note that $\omega_p(\mathbf{r})$ and $\omega_0(\mathbf{r})$ are the plasma and resonant frequencies of a Lorentz oscillator located at $\mathbf{r}$. Then Hamilton's equations of motion (EoMs) can be explicitly written as [20]

$$\begin{aligned} \frac{\partial \mathbf{A}}{\partial t} &= \frac{\delta H}{\delta \mathbf{\Pi}_{AP}} = \frac{1}{\epsilon_0} (\mathbf{\Pi}_{AP} + \mathbf{P}), \\ \frac{\partial \mathbf{\Pi}_{AP}}{\partial t} &= -\frac{\delta H}{\delta \mathbf{A}} = -\nabla \times \frac{1}{\mu_0} \nabla \times \mathbf{A} + \epsilon_0 \nabla \frac{1}{\chi_0} \nabla \cdot \epsilon_0 \mathbf{A}, \\ \frac{\partial \Phi}{\partial t} &= -\frac{\delta H}{\delta \Pi_\Phi} = \frac{1}{\chi_0} \Pi_\Phi, \\ \frac{\partial \Pi_\Phi}{\partial t} &= \frac{\delta H}{\delta \Phi} = \nabla \cdot \epsilon_0 \nabla \Phi - \nabla \cdot \mathbf{P}, \\ \frac{\partial \mathbf{P}}{\partial t} &= \frac{\delta H}{\delta \mathbf{\Pi}_P} = \frac{\epsilon_0}{\beta(\mathbf{r})} \mathbf{\Pi}_P, \\ \frac{\partial \mathbf{\Pi}_P}{\partial t} &= -\frac{\delta H}{\delta \mathbf{P}} = -\frac{1}{\epsilon_0} \mathbf{\Pi}_{AP} - \frac{f(\mathbf{r}) + 1}{\epsilon_0} \mathbf{P} - \nabla \Phi. \end{aligned} \tag{6}$$

Defining generalized position and momentum for the whole system as

$$\mathbf{q} \triangleq [\mathbf{A}, \Phi, \mathbf{P}]^T, \quad \mathbf{p} \triangleq [\mathbf{\Pi}_{AP}, -\Pi_\Phi, \mathbf{\Pi}_P]^T, \tag{7}$$

one can compactly write the above Hamiltonian in a block matrix form as

$$H = \frac{1}{2} \int_V d\mathbf{r} \begin{bmatrix} \mathbf{q} \\ \mathbf{p} \end{bmatrix}^\dagger \cdot \begin{bmatrix} \overline{\mathbf{K}} & \overline{\mathbf{C}} \\ \overline{\mathbf{C}}^\dagger & \overline{\mathbf{M}} \end{bmatrix} \cdot \begin{bmatrix} \mathbf{q} \\ \mathbf{p} \end{bmatrix}, \tag{8}$$

where each block matrix can be explicitly written by

$$\overline{\mathbf{K}} = \left[\begin{array}{c|c|c} \nabla \times \frac{1}{\mu_0} \nabla \times -\epsilon_0 \cdot \nabla \frac{1}{\chi_0} \nabla \cdot \epsilon_0 & 0 & 0 \\ \hline 0 & \nabla \cdot \epsilon_0 \nabla & -\nabla \cdot \\ \hline 0 & \nabla & \frac{f(\mathbf{r})+1}{\epsilon_0} \end{array}\right],$$

$$\overline{\mathbf{C}} = \left[\begin{array}{c|c|c} 0 & 0 & 0 \\ \hline 0 & 0 & 0 \\ \hline \frac{1}{\epsilon_0} & 0 & 0 \end{array}\right], \quad \overline{\mathbf{M}} = \left[\begin{array}{c|c|c} \frac{1}{\epsilon_0} & 0 & 0 \\ \hline 0 & -\frac{1}{\chi_0} & 0 \\ \hline 0 & 0 & \frac{\beta(\mathbf{r})}{\epsilon_0} \end{array}\right]. \tag{9}$$

Note that, in the block matrix representation, the partitions are delimited by solid vertical and horizontal lines. The Hamilton's EoMs can be written in the block matrix form (see its details in Appendix A) as

$$\frac{\partial}{\partial t} \begin{bmatrix} \mathbf{q} \\ \mathbf{p} \end{bmatrix} = \begin{bmatrix} \overline{\mathbf{C}}^\dagger & \overline{\mathbf{M}} \\ -\overline{\mathbf{K}} & -\overline{\mathbf{C}} \end{bmatrix} \begin{bmatrix} \mathbf{q} \\ \mathbf{p} \end{bmatrix}. \tag{10}$$

However, the Hamilton's EoMs may not be simply converted to a Hermitian eigenvalue problem due to the presence of $\overline{\mathbf{C}}$ (cross-coupling term), as discussed in Appendix B in detail.

B. Generalized Hermitian eigenvalue problem

To derive a simpler standard Hermitian eigenvalue problem, we redefine generalized position and momentum such as

$$\mathbf{q} \triangleq [\mathbf{A}, \Pi_\Phi, \mathbf{\Pi}_P]^T, \quad \mathbf{p} \triangleq [\mathbf{\Pi}_{AP}, \Phi, -\mathbf{P}]^T, \tag{11}$$

motivated by the cross-coupling term $\overline{\mathbf{C}}$. It still preserves the structure of the original Hamiltonian density $\mathcal{H}(\mathbf{r}, t)$ in Eq. (5), i.e.,

$$H = \frac{1}{2} \int_V d\mathbf{r} \begin{bmatrix} \mathbf{q} \\ \mathbf{p} \end{bmatrix}^\dagger \cdot \begin{bmatrix} \overline{\mathbf{K}} & \overline{\mathbf{0}} \\ \overline{\mathbf{0}} & \overline{\mathbf{M}} \end{bmatrix} \cdot \begin{bmatrix} \mathbf{q} \\ \mathbf{p} \end{bmatrix}, \tag{12}$$

where the "spring constant" and "mass" matrices are also redefined as

$$\overline{\mathbf{K}} = \left[\begin{array}{c|c|c} \nabla \times \frac{1}{\mu_0} \nabla \times -\epsilon_0 \nabla \frac{1}{\chi_0} \nabla \cdot \epsilon_0 & 0 & 0 \\ \hline 0 & -\frac{1}{\chi_0} & 0 \\ \hline 0 & 0 & \frac{\beta(\mathbf{r})}{\epsilon_0} \end{array}\right], \tag{13}$$

$$\overline{\mathbf{M}} = \left[\begin{array}{c|c|c} \frac{1}{\epsilon_0} & 0 & \frac{1}{\epsilon_0} \\ \hline 0 & \nabla \cdot \epsilon_0 \nabla & -\nabla \cdot \\ \hline \frac{1}{\epsilon_0} & \nabla & \frac{f(\mathbf{r})+1}{\epsilon_0} \end{array}\right]. \tag{14}$$

As a result, Hamilton's EoMs can be rewritten as

$$\frac{\partial}{\partial t} \begin{bmatrix} \mathbf{q} \\ \mathbf{p} \end{bmatrix} = \begin{bmatrix} \overline{\mathbf{0}} & \overline{\mathbf{M}} \\ -\overline{\mathbf{K}} & \overline{\mathbf{0}} \end{bmatrix} \cdot \begin{bmatrix} \mathbf{q} \\ \mathbf{p} \end{bmatrix}. \tag{15}$$

Thus, one can derive EoMs only for the generalized $\mathbf{q}$ or $\mathbf{p}$ variable involving a second-order time derivative. For instance, for the $\mathbf{q}$ case,

$$\frac{\partial^2}{\partial t^2} \mathbf{q} = \overline{\mathbf{M}} \cdot (-\overline{\mathbf{K}}) \cdot \mathbf{q}. \tag{16}$$

Since $\overline{\mathbf{M}}$ and $\overline{\mathbf{K}}$ are both positive-definite and Hermitian, the above is convertible to an explicit GH-EVP as

$$\omega^2 \overline{\mathbf{M}}^{-1} \cdot \tilde{\mathbf{q}}_{\omega,\lambda}(\mathbf{r}) = \overline{\mathbf{K}} \cdot \tilde{\mathbf{q}}_{\omega,\lambda}(\mathbf{r}), \tag{17}$$

where $\tilde{\mathbf{q}}_{\omega,\lambda}(\mathbf{r})$ is a time-harmonic eigenmode of $\mathbf{q}(\mathbf{r}, t)$ and ω is eigenfrequency. Note that the above GH-EVP is equivalent to Eq. (14) in Ref. [5], as proven in Appendix C. As

a result, one can expand the generalized position in terms of time-harmonic eigenmodes

$$\mathbf{q}(\mathbf{r},t)=\int_{\Omega_+}d\omega\sum_{\lambda}\tilde{\mathbf{q}}_{\omega,\lambda}(\mathbf{r})\underbrace{d_{\omega,\lambda}e^{-i\omega t}}_{d_{\omega,\lambda}(t)}+\text{H.c.},\tag{18}$$

where Ω_+ denotes the set of positive eigenfrequencies and λ denotes comprehensive degeneracy index for EM fields and Lorentz oscillators.

C. Diagonalization of Hamiltonian

The GH-EVP inherently possesses the following two orthonormal conditions:

$$\int_V d\mathbf{r}\ (\tilde{\mathbf{q}}^{\dagger}_{\omega,\lambda}\cdot\overline{\mathbf{M}}^{-1}\cdot\tilde{\mathbf{q}}_{\omega',\lambda'})=\delta_{\omega,\omega'}\delta_{\lambda,\lambda'},\tag{19}$$

$$\int_V d\mathbf{r}\ (\tilde{\mathbf{q}}^{\dagger}_{\omega,\lambda}\cdot\overline{\mathbf{K}}\cdot\tilde{\mathbf{q}}_{\omega',\lambda'})=\omega^2\delta_{\omega,\omega'}\delta_{\lambda,\lambda'}.\tag{20}$$

Substituting (18) into (12) and using the above orthonormal conditions, one can diagonalize the Hamiltonian as

$$H=\frac{1}{2}\int_{\Omega_+}d\omega\sum_{\lambda}\omega^2(d^*_{\omega,\lambda}d_{\omega,\lambda}+d_{\omega,\lambda}d^*_{\omega,\lambda}).\tag{21}$$

The detailed procedure can be found in Appendix D.

Note that the present diagonalization procedure shall be called *no-cross-coupling description* since we remove the cross-coupling term $\overline{\mathbf{C}}$ by properly redefining generalized position and momentum. We also present another diagonalization strategy, called *cross-coupling description*, even in the presence of the cross-coupling term, in Appendix E. It turns out that the latter has a twice-larger linear system; thus, the no-cross-coupling description here is more computationally efficient.

III. QUANTIZATION BY MODE DECOMPOSITION

The subsequent quantization procedure becomes straightforward with the use of time-harmonic eigenmodes [3,10]. Let us elevate the conjugate pairs into operators:

$$\mathbf{q}(\mathbf{r},t)\rightarrow\hat{\mathbf{q}}(\mathbf{r},t),\quad \mathbf{p}(\mathbf{r},t)\rightarrow\hat{\mathbf{p}}(\mathbf{r},t),\tag{22}$$

which satisfy canonical commutator relations

$$[[\hat{\mathbf{q}}(\mathbf{r},t)]_i,[\hat{\mathbf{p}}(\mathbf{r}',t)]_j]=i\hbar\delta(\mathbf{r}-\mathbf{r}')\delta_{i,j}\hat{I},\tag{23}$$

$$[[\hat{\mathbf{q}}(\mathbf{r},t)]_i,[\hat{\mathbf{q}}(\mathbf{r}',t)]_j]=[[\hat{\mathbf{p}}(\mathbf{r},t)]_i,[\hat{\mathbf{p}}(\mathbf{r}',t)]_j]=0,\tag{24}$$

for $i,j\in\{1,2,\ldots,7\}$ including three-dimensional vector components of vector potential and polarization density and scalar potential (and their conjugate pairs). Note that $[\hat{\mathbf{q}}(\mathbf{r},t)]_i$ [or $[\hat{\mathbf{p}}(\mathbf{r}',t)]_j$] stands for ith element of $\mathbf{q}(\mathbf{r},t)$ [or the jth element of $\mathbf{p}(\mathbf{r},t)$]. Annihilation and creation operators can be defined by simply elevating modal amplitudes scaled by $\sqrt{\hbar/\omega}$ as

$$d_{\omega,\lambda}(t)\rightarrow\sqrt{\frac{\hbar}{\omega}}\hat{d}_{\omega,\lambda}(t),\quad d^*_{\omega,\lambda}(t)\rightarrow\sqrt{\frac{\hbar}{\omega}}\hat{d}^{\dagger}_{\omega,\lambda}(t),\tag{25}$$

which also satisfies the bosonic commutator relations:

$$[\hat{d}_{\omega,\lambda},\hat{d}^{\dagger}_{\omega',\lambda'}]=\delta_{\omega,\omega'}\delta_{\lambda,\lambda'}\hat{I},\tag{26}$$

$$[\hat{d}_{\omega,\lambda},\hat{d}_{\omega',\lambda'}]=0=[\hat{d}^{\dagger}_{\omega,\lambda},\hat{d}^{\dagger}_{\omega',\lambda'}].\tag{27}$$

Thus, the resulting observables are represented by

$$\hat{\mathbf{q}}(\mathbf{r},t)=\int_{\Omega_+}d\omega\sum_{\lambda}\tilde{\mathbf{q}}_{\omega,\lambda}(\mathbf{r})\sqrt{\frac{\hbar}{\omega}}\underbrace{\hat{d}_{\omega,\lambda}e^{-i\omega t}}_{\hat{d}_{\omega,\lambda}(t)}+\text{H.c.}\tag{28}$$

One can easily check the consistency between canonical commutator relations and bosonic commutator relations by substituting (28) into the left-hand sides (LHSs) of (23) and (24), using the orthonormal properties of time-harmonic eigenmodes, and showing that the resulting LHSs of (23) and (24) become the right-hand sides (RHSs) of (23) and (24).

Finally, the Hamiltonian operator, the quantum equivalence of (21) that has been elevated to become a quantum operator, can be diagonalized with respect to the ladder operators for both descriptions as

$$\hat{H}=\int_{\Omega_+}d\omega\sum_{\lambda}\hbar\omega\left(\hat{d}^{\dagger}_{\omega,\lambda}\hat{d}_{\omega,\lambda}+\frac{1}{2}\hat{I}\right),\tag{29}$$

where the zero-point energy becomes $E_0=\int_{\Omega_+}d\omega\sum_{\lambda}\hbar\omega/2$. An eigenstate of the corresponding time-independent (stationary) quantum state Eq. (2) is the multimode-Fock state. In a word, the Hamiltonian has been decomposed into a sum of Hamiltonians of independent harmonic oscillators. The eigenstate of each individual Hamiltonian is its respective Fock state. This physical picture is similar to the quantization of electromagnetic field in vacuum using Fourier mode decomposition. But here we have used numerically-sought-for modes using CEM rather than Fourier modes. It should also be noted that this eigenstate does not represent bare eigenstate for neither free EM field nor polarization density but a dressed state which combines the coupling between them. In a word, the free field modes have been "dressed" by the matter modes, and vice versa.

IV. NUMERICAL SOLUTIONS TO THE GENERALIZED HERMITIAN EIGENVALUE PROBLEM

Solving the GH-EVPs in (17) returns the uncountably infinite set of eigenmodes, which is impossible in practice. Furthermore, analytic solutions of (17) may not exist in general. To remedy this, one can use computational electromagnetic (CEM) methods which can be viewed as a subspace projection method [21]. Here, we refer subspace projection method to a general procedure to approximate an infinite-dimensional solution space $\mathcal{V}$ by a finite-dimensional (countably finite) one $\mathcal{V}_d$.[1] As a consequence, (17), as is commonly done in numerical linear algebra [23], becomes a finite-dimensional linear system such as

$$\overline{\mathbf{M}}_d^{-1}\cdot\overline{\mathbf{\Psi}}_d\cdot\overline{\boldsymbol{\omega}}_d^2=\overline{\mathbf{K}}_d\cdot\overline{\mathbf{\Psi}}_d,\tag{30}$$

[1]Note that the term subspace projection method (also known as Krylov subspace methods) [22] is also used in the numerical linear algebra field, referring to a procedure to deal efficiently with large linear systems.

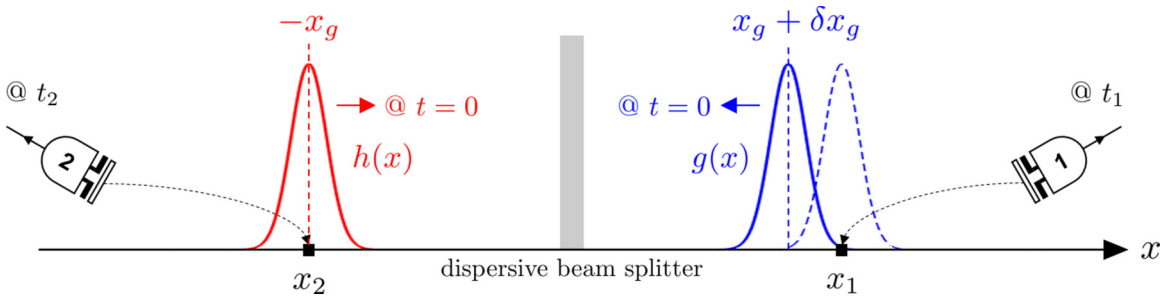

FIG. 2. Schematic of 1-D simulations for the HOM effect in a dispersive beam splitter. A nonentangled photon pair is initially localized around x_g and $-x_g$ and sent to a beam splitter. After the interference, we measure the second-order correlation at (x_1, t_1) and (x_2, t_2) by perturbing the initialization position (δx_g) of the photon initialized on the right side.

where the subscript d stands for the approximation by subspace projection method; $\overline{\mathbf{M}}_d$ and $\overline{\mathbf{K}}_d$ are discrete counterparts of $\overline{\mathbf{M}}$ and $\overline{\mathbf{K}}$, $\overline{\boldsymbol{\omega}}_d$ is a diagonal matrix whose elements are eigenfrequencies including degeneracy, and $\overline{\boldsymbol{\Psi}}_d$ is a matrix that collects all numerical time-harmonic eigenmodes. If the dimension of the solution space $\mathcal{V}_d$ was N, the size of $\overline{\mathbf{M}}_d$, $\overline{\mathbf{K}}_d$, $\overline{\boldsymbol{\omega}}_d$, and $\overline{\boldsymbol{\Psi}}_d$ would be $N \times N$. Most subspace projection methods employ a mesh on which continuum solutions are sampled by finite number. The dimension of the solution space is closely related to the mesh size. The continuum eigenmode index (ω, λ) is replaced by a single index n which represents nth numerical time-harmonic eigenmodes $[\overline{\boldsymbol{\Psi}}_d]_{:,n}$ having nth eigenfrequency $[\overline{\boldsymbol{\omega}}_d]_{n,n} = \omega_n$. Note that an element in the ith row and nth column of $\overline{\boldsymbol{\Psi}}_d$, i.e., $[\overline{\boldsymbol{\Psi}}_d]_{i,n}$, represents the nth numerical time-harmonic eigenmode sampled at the ith grid point.

V. NUMERICAL EXAMPLES

In this section, we discuss two numerical studies using the proposed quantization scheme: (1) the Hong-Ou-Mandel (HOM) effect [24] in a one-dimensional (1-D) dispersive beam splitter, and (2) nonlocal dispersion cancellation (NLDC) for an energy-time entangled photon pair [25].

Note that these are 1-D simulations in which the vector potential $\mathbf{A}$ is always transverse (polarized along the z axis) to the propagation direction (x axis) while the polarization density is also transverse. Hence, one can use the Lorenz gauge with $\Phi = \Pi_\Phi = 0$, which is equivalent to the Coulomb gauge. And, (17) is to be modified accordingly. As a result, the resulting dynamical variables are $\mathbf{A}(\mathbf{r}, t) = \hat{z}A(x, t)$, $\mathbf{\Pi}_{AP}(\mathbf{r}, t) = \hat{z}\Pi_{AP}(x, t)$, $\mathbf{P}(\mathbf{r}, t) = \hat{z}P(x, t)$, and $\mathbf{\Pi}_P(\mathbf{r}, t) = \Pi_P(x, t)$.

A. Hong-Ou-Mandel effect in dispersive beam splitter

Here, we discuss 1-D simulation results of the HOM effect [24] in a dispersive beam splitter.

The problem geometry is illustrated in Fig. 2. The problem domain $V \in \{x \in [-L/2, L/2]\}$, which is the free space, includes the dielectric slab in the middle with thickness L_s. Then, a nonentangled photon pair is initialized ($t = 0$) around $x_1 = x_g$ and $x_2 = -x_g$ in the free space and sent to a beam splitter. Each photon is assumed to be polychromatic, riding on a Gaussian wave packet. After the interference, we measure the second-order correlation at (x_1, t_1) and (x_2, t_2) by perturbing the initialization position of the photon on the right side, i.e., $x_1 = x_g + \delta x_g$. The beam splitter is assumed to be made of a single dielectric slab, which is modeled by filling Lorentz oscillators to account for dispersion effects. Simulation parameters, design of the beam splitter, relevant numerical setup, and modeling incoming polychromatic photons are discussed in detail in Appendix F.

Figure 3 shows the second-order correlation versus τ for various ω_p. The smaller ω_p, the more dispersive the beam splitter becomes. Note that the dispersionless case was calculated based on the CQ-NMD for inhomogeneous and dispersionless media [3].

The almost zero coincidence when $\tau = 0$ is the clear evidence of the creation of path-entangled photons, i.e., $N00N$ states where $N = 2$. This results from the perfect destructive interference between the two photons inside the 50 : 50 beam splitter [26–28]. When $\tau \neq 0$, the temporal decoherence—different arrival times of the incident photons to the beam

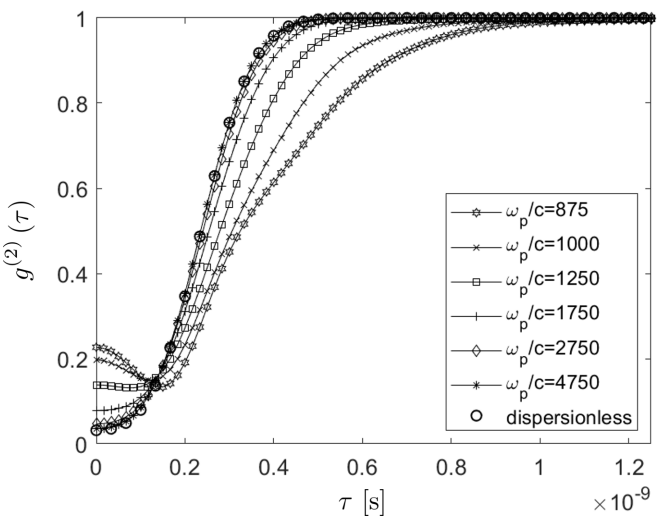

FIG. 3. Second-order correlation versus time delay $[g^{(2)}(\tau)]$ for various ω_p. When $\tau = 0$, dispersion degrades the perfect destructive interference between two incident photons; consequently, $g^{(2)}(\tau)$ increases depending on the dispersion degree. In contrast, when $\tau \neq 0$, dispersion can mitigate the time-harmonic decoherence such that $g^{(2)}(\tau)$ is slightly lower than the dispersionless case.

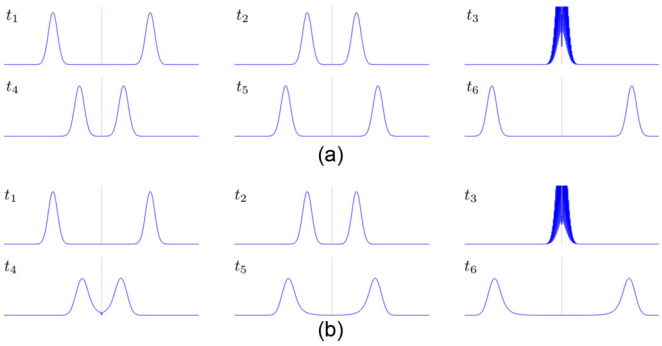

FIG. 4. Time evolution of the energy density expectation value when $\tau = 0$ for (a) $\omega_p/c = 4750$ and (b) $\omega_p/c = 875$. The former is almost dispersionless whereas the latter is highly dispersive. Accordingly, one can observe the deformation of wave packets in the latter case due to the group-velocity dispersion while passing the beam splitter.

splitter—degrades the perfect destructive interference; consequently, $g^{(2)}$ gradually increases as τ gets larger.

In the presence of dispersion, even when $\tau = 0$, two polychromatic photons cannot have perfect destructive interference over their whole bandwidth. This is because the dispersive beam splitter quickly loses the 50 : 50 performance as an operating frequency deviates from the carrier frequency of photons. In other words, the 50 : 50 performance bandwidth becomes much narrower than the photon's bandwidth depending on the dispersion extent; hence, $g^{(2)}$ increases. It is interesting to observe that when $\tau \neq 0$, $g^{(2)}$ for dispersive cases gets lower than that of the dispersionless case. This is because the dispersion effects can mitigate the degradation by the temporal decoherence. More specifically, the interaction time between photons and the dispersive beam splitter becomes longer than the dispersionless case so that photons can stay longer in the dispersive beam splitter. As a result, the partial destructive interference can happen even though the arrival times of incidence photons are mismatched. This is the hallmark of dispersion effects, viz., the decrease of the quality factor of the HOM dip, and our simulation correctly captures this effect.

To show this, Fig. 4 compares the time evolution of the energy density expectation value for $\omega_p/c = 4750$ and $\omega_p/c = 875$, which correspond to almost dispersionless and highly dispersive cases, respectively. One can observe the deformation of the wave packets after passing the dispersive beam splitter, compared with the dispersionless case. This is because the chromatic dispersion changes the group velocity of the wave packets during interacting with the dispersive beam splitter.

B. Nonlocal dispersion cancellation

Unlike to classical EM pulses, an energy-time entangled photon pair can cancel the dispersion effects in the nonlocal sense, called *nonlocal dispersion cancellation* (NLDC). This is another nonclassical feature of entangled photons, first proposed by Franson [25]. More specifically, even if signal and idler photons experience dispersion effects independently on their own path, the degree of coincidence can be maintained as if there are no dispersive media. Thus, it has a great promise in resolving entanglement loss that significantly degrades the system performance of quantum communication technology. Recently, several experimental works have been performed [29] to validate the NLDC effect even for a few tens of kilometers [30]. Here, we conduct numerical experiments to confirm the NLDC effect via the proposed quantization scheme.

Again, we consider a 1-D problem geometry, as illustrated in Fig. 5. An energy-time entangled photon pair is initialized at $x = 0$ and signal and idler photons are supposed to propagate to the right and left sides, respectively. Again, each photon is polychromatic. We place a dispersive medium on each photon's path, denoted by β_r and β_l, where β represents a second-order dispersion of the medium. The degree of coincidence is computed from two photodetections at (x_1, t_1) and (x_2, t_2). We present simulation parameters, numerical setup, design of dispersive media, and modeling the energy-time entangled photons in Appendix G in detail.

Note that we again use the FDM with Bloch-Floquet boundary conditions to solve (17).

We conducted four simulations for both entangled and nonentangled photons: (1) free space (no dispersive media), (2) in the presence of left dispersive media (β_l), (3) right dispersive media (β_r), and (4) both dispersive media (β_l and β_r). Then, we computed two-time coincidences for all cases. Figure 6 displays aggregate coincidence (normalized by the free-space case) versus time difference τ, defined by $\tau = (t_1 - \tilde{t}_1) - (t_2 - \tilde{t}_2)$. Here, $\tilde{t}_i$ denotes a delay of the ith photon arrival time to the ith photodetector for $i = 1, 2$, compared with the free-space case. Note that the delay is mostly affected by the degree of the first-order dispersion α [29].

For the entangled photon pair in Fig. 6(a), the presence of either left or right dispersive media gets the coincidence peak broadened compared with the free-space case. Furthermore, since both left and right dispersive media have the same magnitude of second-order dispersion, the broadening amounts are almost equal. It is very interesting to observe that, when both dispersive media are present, the coincidence curve becomes narrower, resulting from the destructive interference of the second-order dispersion. However, due to imperfect cancellations in higher-order dispersions, the coincidence peak is not perfectly converging to the free-space case [31]. On the other hand, as observed in Fig. 6(b), the nonentangled photon pairs do not exhibit any dispersion cancellation that the coincidence curve in the presence of both dispersive media gets wider than one-sided medium cases.

VI. CONCLUSION

We have presented a mathematical modeling approach, called *canonical quantization with numerical mode decomposition*, suited for studying how incoming photons interact with finite-sized dispersive media which may not be simply described by the previous Fano-diagonalization-based quantization methods. The main procedure was to (1) inspect a system where electromagnetic (EM) fields are coupled to nonuniformly distributed Lorentz oscillators in Hamiltonian mechanics, (2) derive a generalized Hermitian eigenvalue problem for conjugate pairs in Euclidean space,

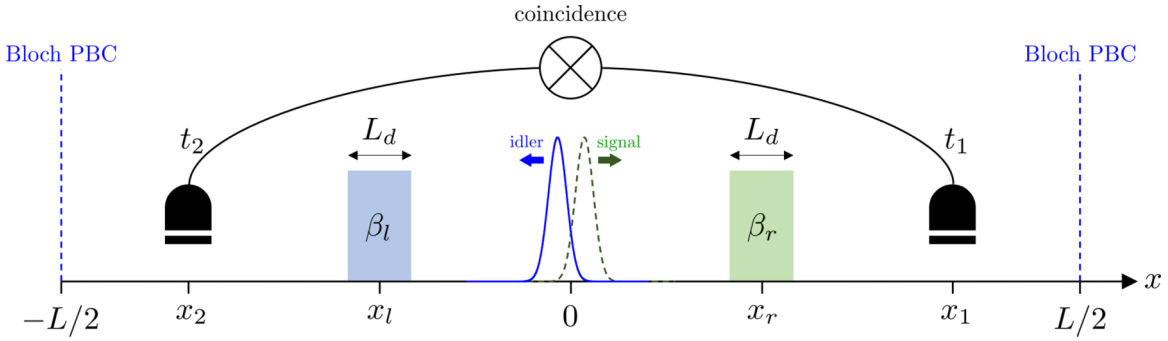

FIG. 5. Problem geometry of 1-D simulations to observe nonlocal dispersion cancellation. An energy-time entangled (or nonentangled) photon pair is initialized at $x = 0$ and the signal and idler photons are supposed to propagate to the right and left sides, respectively. We place a dispersive medium on each photon's path, denoted by β_r and β_l, where β represents a second-order dispersion of the medium. The degree of coincidence is computed from two photodetections at (x_1, t_1) and (x_2, t_2).

(3) apply computational electromagnetics methods to find a countably finite set of time-harmonic eigenmodes which diagonalizes the Hamiltonian, and (4) perform the subsequent canonical quantization with mode decomposition. Moreover, we have provided several numerical simulations for fully-quantum-theoretic phenomena, not predictable by the classical Maxwell's equations, such as nonlocal dispersion cancellation of an entangled photon pair and the Hong-Ou-Mandel (HOM) effect in a dispersive beam splitter, showing the great promise of the CEM-driven QEM/QO research. We have shown the equivalence between the present approach and the recent works [4,5] by the Jauslin's group, although, our formulation was based on Euclidean space with the use of CEM methods rather than reciprocal space.

In the future, we will compare the computational efficiency of the present and Jauslin's group's formulations for various cases. Furthermore, we will extend the present approach to dissipative quantum systems by introducing coarse-grained bath oscillators. Moreover, we will investigate how to remove the redundancy when using Lorenz gauge, which is important to account for trapped modes, such as surface-plasmon polaritons.

ACKNOWLEDGMENTS

This work is funded by National Science Foundation Grant No. 1818910 and a startup fund at Purdue University. W. C. Chew is also funded by Distinguished Visiting Scholars Scheme (DVSS) at the University of Hong Kong (HKU), 2019.

APPENDIX A: HAMILTON'S EQUATIONS OF MOTION IN BLOCK MATRIX FORM

Hamilton's EoMs can be expressed in the block matrix form as

$$\frac{\partial}{\partial t}\begin{bmatrix}\mathbf{q}\\ \mathbf{p}\end{bmatrix} = \begin{bmatrix}\frac{\delta H}{\delta \mathbf{p}}\\ -\frac{\delta H}{\delta \mathbf{q}}\end{bmatrix} = \overline{\mathbf{J}}\cdot\begin{bmatrix}\frac{1}{\delta \mathbf{q}}\\ \frac{1}{\delta \mathbf{p}}\end{bmatrix}\delta H, \tag{A1}$$

where the differential Hamiltonian is given by

$$\begin{aligned}\delta H &= \frac{1}{2}\int_V d\mathbf{r}\begin{bmatrix}\delta\mathbf{q}\\ \delta\mathbf{p}\end{bmatrix}^\dagger\cdot\overline{\mathbf{U}}\cdot\begin{bmatrix}\mathbf{q}\\ \mathbf{p}\end{bmatrix} + \begin{bmatrix}\mathbf{q}\\ \mathbf{p}\end{bmatrix}^\dagger\cdot\overline{\mathbf{U}}\cdot\begin{bmatrix}\delta\mathbf{q}\\ \delta\mathbf{p}\end{bmatrix}\\ &= \int_V d\mathbf{r}\begin{bmatrix}\delta\mathbf{q}\\ \delta\mathbf{p}\end{bmatrix}^\dagger\cdot\overline{\mathbf{U}}\cdot\begin{bmatrix}\mathbf{q}\\ \mathbf{p}\end{bmatrix},\\ \overline{\mathbf{U}} &= \begin{bmatrix}\overline{\mathbf{K}} & \overline{\mathbf{C}}\\ \overline{\mathbf{C}}^\dagger & \overline{\mathbf{M}}\end{bmatrix},\quad \overline{\mathbf{J}} = \begin{bmatrix}\overline{\mathbf{0}} & \overline{\mathbf{I}}\\ -\overline{\mathbf{I}} & \overline{\mathbf{0}}\end{bmatrix},\end{aligned} \tag{A2}$$

and $\overline{\mathbf{I}}$ is an identity matrix.

Substituting the above differential Hamiltonian into (A1) yields

$$\begin{aligned}\frac{\partial}{\partial t}\begin{bmatrix}\mathbf{q}\\ \mathbf{p}\end{bmatrix} &= \overline{\mathbf{J}}\cdot\begin{bmatrix}\frac{1}{\delta\mathbf{q}}\\ \frac{1}{\delta\mathbf{p}}\end{bmatrix}\cdot\left(\int_V d\mathbf{r}\begin{bmatrix}\delta\mathbf{q}\\ \delta\mathbf{p}\end{bmatrix}^\dagger\cdot\overline{\mathbf{U}}\cdot\begin{bmatrix}\mathbf{q}\\ \mathbf{p}\end{bmatrix}\right)\\ &= \overline{\mathbf{J}}\cdot\left(\int_V d\mathbf{r}\begin{bmatrix}\frac{1}{\delta\mathbf{q}}\\ \frac{1}{\delta\mathbf{p}}\end{bmatrix}\cdot\begin{bmatrix}\delta\mathbf{q}\\ \delta\mathbf{p}\end{bmatrix}^\dagger\cdot\overline{\mathbf{U}}\cdot\begin{bmatrix}\mathbf{q}\\ \mathbf{p}\end{bmatrix}\right).\end{aligned} \tag{A3}$$

One can make the use of the properties of functional derivatives [10,32–34], as a result,

$$\begin{aligned}\begin{bmatrix}\frac{1}{\delta\mathbf{q}(\mathbf{r}',t)}\\ \frac{1}{\delta\mathbf{p}(\mathbf{r}',t)}\end{bmatrix}\cdot\begin{bmatrix}\delta\mathbf{q}(\mathbf{r},t)\\ \delta\mathbf{p}(\mathbf{r},t)\end{bmatrix}^\dagger &= \begin{bmatrix}\frac{\delta\mathbf{q}(\mathbf{r},t)}{\delta\mathbf{q}(\mathbf{r}',t)} & \frac{\delta\mathbf{p}(\mathbf{r},t)}{\delta\mathbf{q}(\mathbf{r}',t)}\\ \frac{\delta\mathbf{q}(\mathbf{r},t)}{\delta\mathbf{p}(\mathbf{r}',t)} & \frac{\delta\mathbf{p}(\mathbf{r},t)}{\delta\mathbf{p}(\mathbf{r}',t)}\end{bmatrix}\\ &= \begin{bmatrix}\overline{\boldsymbol{\delta}}(\mathbf{r}-\mathbf{r}') & 0\\ 0 & \overline{\boldsymbol{\delta}}(\mathbf{r}-\mathbf{r}')\end{bmatrix}.\end{aligned} \tag{A4}$$

Upon applying the sifting property of the δ function, the resulting Hamilton's EoMs become

$$\begin{aligned}\frac{\partial}{\partial t}\begin{bmatrix}\mathbf{q}\\ \mathbf{p}\end{bmatrix} &= \left(\int_V d\mathbf{r}\begin{bmatrix}0 & \overline{\boldsymbol{\delta}}(\mathbf{r}-\mathbf{r}')\\ -\overline{\boldsymbol{\delta}}(\mathbf{r}-\mathbf{r}') & 0\end{bmatrix}\cdot\overline{\mathbf{U}}\cdot\begin{bmatrix}\mathbf{q}\\ \mathbf{p}\end{bmatrix}\right)\\ &= \overline{\mathbf{J}}\cdot\overline{\mathbf{U}}\cdot\begin{bmatrix}\mathbf{q}\\ \mathbf{p}\end{bmatrix} = \begin{bmatrix}\overline{\mathbf{C}}^\dagger & \overline{\mathbf{M}}\\ -\overline{\mathbf{K}} & -\overline{\mathbf{C}}\end{bmatrix}\cdot\begin{bmatrix}\mathbf{q}\\ \mathbf{p}\end{bmatrix}.\end{aligned} \tag{A5}$$

The above procedure was also applied to arriving at (15).

APPENDIX B: NON-HERMITICITY OF THE EIGENVALUE PROBLEM DUE TO CROSS-COUPLING TERMS

Let us represent the dynamical variables by the linear superposition of time-harmonic eigenmodes as

$$\begin{bmatrix}\mathbf{q}\\ \mathbf{p}\end{bmatrix} = \int_\Omega d\omega\sum_\lambda\left(\begin{bmatrix}\tilde{\mathbf{q}}_{\omega,\lambda}(\mathbf{r})\\ \tilde{\mathbf{p}}_{\omega,\lambda}(\mathbf{r})\end{bmatrix}\underbrace{c_{\omega,\lambda}e^{-i\omega t}}_{c_{\omega,\lambda}(t)}\right), \tag{B1}$$

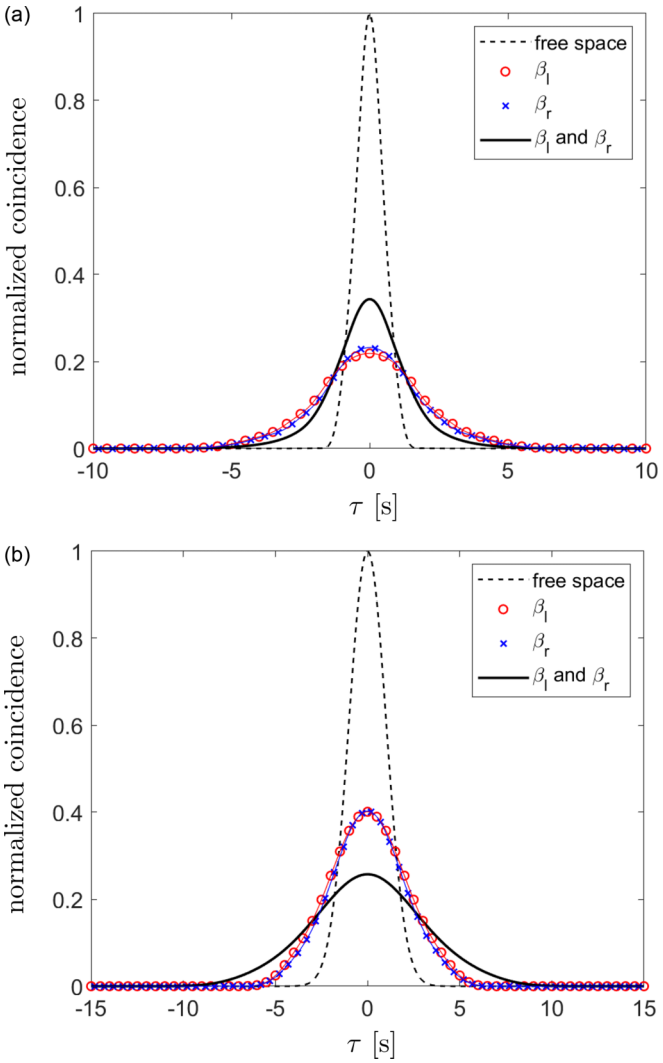

FIG. 6. Coincidence versus time difference τ for (a) entangled and (b) nonentangled photon pairs. Note that $\tau = (t_1 - \tilde{t}_1) - (t_2 - \tilde{t}_2)$ where $\tilde{t}_i$ is the delay of arrival time of th ith photon to the photodetector.

where Ω denotes a set including both positive and negative eigenfrequencies. By substituting (B1) into (10) and replacing the time derivative by $-i\omega$, one arrives at

$$\omega \begin{bmatrix} \tilde{\mathbf{q}}_{\omega,\lambda} \\ \tilde{\mathbf{p}}_{\omega,\lambda} \end{bmatrix} = i\overline{\mathbf{J}} \cdot \overline{\mathbf{U}} \cdot \begin{bmatrix} \tilde{\mathbf{q}}_{\omega,\lambda} \\ \tilde{\mathbf{p}}_{\omega,\lambda} \end{bmatrix}. \tag{B2}$$

However, since $i\overline{\mathbf{J}} \cdot \overline{\mathbf{U}}$ is a non-Hermitian matrix, solutions of (B2) may not ensure the completeness of time-harmonic eigenmodes nor the realness of the eigenfrequencies.

APPENDIX C: EQUIVALENCE BETWEEN THE PRESENT FORMULATION AND REF. [5]

From the no-cross-coupling description, we can apply the canonical transformation for generalized position and momentum as

$$\mathbf{q}' = \overline{\mathbf{M}}^{-\frac{1}{2}} \cdot \mathbf{q}, \quad \mathbf{p}' = \overline{\mathbf{M}}^{\frac{1}{2}} \cdot \mathbf{p}. \tag{C1}$$

Then, the Hamiltonian (12) can be brought to the form

$$\begin{aligned} H &= \frac{1}{2}\int_V d\mathbf{r} \begin{bmatrix} \mathbf{q} \\ \mathbf{p} \end{bmatrix}^\dagger \cdot \begin{bmatrix} \overline{\mathbf{K}} & \overline{\mathbf{0}} \\ \overline{\mathbf{0}} & \overline{\mathbf{M}} \end{bmatrix} \cdot \begin{bmatrix} \mathbf{q} \\ \mathbf{p} \end{bmatrix} \\ &= \frac{1}{2}\int_V d\mathbf{r} \begin{bmatrix} \mathbf{q}' \\ \mathbf{p}' \end{bmatrix}^\dagger \cdot \begin{bmatrix} \overline{\mathbf{M}}^{\frac{1}{2}} \cdot \overline{\mathbf{K}} \cdot \overline{\mathbf{M}}^{\frac{1}{2}} & \overline{\mathbf{0}} \\ \overline{\mathbf{0}} & \overline{\mathbf{I}} \end{bmatrix} \cdot \begin{bmatrix} \mathbf{q}' \\ \mathbf{p}' \end{bmatrix} \\ &= \frac{1}{2}\int_V d\mathbf{r} (\mathbf{p}')^\dagger \cdot \mathbf{p}' + (\mathbf{q}')^\dagger \cdot \overline{\mathbf{\Omega}}^2 \cdot \mathbf{q}', \end{aligned} \tag{C2}$$

where the positive symmetric operator $\overline{\mathbf{\Omega}}^2 = \overline{\mathbf{M}}^{\frac{1}{2}} \cdot \overline{\mathbf{K}} \cdot \overline{\mathbf{M}}^{\frac{1}{2}}$, called *frequency operator*. Next, we show the equivalence between the GH-EVP (17) and equation (14) in Ref. [5]. The standard eigenvalue problem of equation (14) in Ref. [5] is given by

$$\begin{aligned} \overline{\mathbf{\Omega}}^2 \cdot \boldsymbol{\psi}_{\omega,\lambda} &= \omega^2 \boldsymbol{\psi}_{\omega,\lambda}, \\ \overline{\mathbf{M}}^{\frac{1}{2}} \cdot \overline{\mathbf{K}} \cdot \overline{\mathbf{M}}^{\frac{1}{2}} \cdot \boldsymbol{\psi}_{\omega,\lambda} &= \omega^2 \boldsymbol{\psi}_{\omega,\lambda}, \\ \overline{\mathbf{K}} \cdot \overline{\mathbf{M}}^{\frac{1}{2}} \cdot \boldsymbol{\psi}_{\omega,\lambda} &= \omega^2 \overline{\mathbf{M}}^{-\frac{1}{2}} \cdot \boldsymbol{\psi}_{\omega,\lambda}. \end{aligned} \tag{C3}$$

Identifying $\tilde{\mathbf{q}}_{\omega,\lambda} = \overline{\mathbf{M}}^{\frac{1}{2}} \cdot \boldsymbol{\psi}_{\omega,\lambda}$, the above can be written by

$$\overline{\mathbf{K}} \cdot \tilde{\mathbf{q}}_{\omega,\lambda} = \omega^2 \overline{\mathbf{M}}^{-1} \cdot \tilde{\mathbf{q}}_{\omega,\lambda}. \tag{C4}$$

Thus, our GH-EVP and that in Ref. [5] are mathematically equivalent. It is to be noted that our GH-EVP is based on Euclidean space, although Eq. (14) in Ref. [5] is based on reciprocal space.

APPENDIX D: DIAGONALIZATION OF THE CLASSICAL HAMILTONIAN

The generalized momentum variable can be represented by

$$\mathbf{p} = \int_{\Omega_+} d\omega \sum_\lambda \tilde{\mathbf{p}}_{\omega,\lambda} d_{\omega,\lambda} e^{-i\omega t} + \text{H.c.} \tag{D1}$$

By substituting (18) and (D1) into the original Hamiltonian (12) and rearranging it, one can arrive at

$$\begin{aligned} H = &\frac{1}{2}\int_V d\mathbf{r} \left(\int_{\Omega_+} d\omega \sum_\lambda \tilde{\mathbf{q}}^\dagger_{\omega,\lambda} d^*_{\omega,\lambda} e^{i\omega t} \right) \\ &\cdot \overline{\mathbf{K}} \cdot \left(\int_{\Omega_+} d\omega' \sum_{\lambda'} \tilde{\mathbf{q}}_{\omega',\lambda'} d_{\omega',\lambda'} e^{-i\omega' t} \right) \\ &+ \frac{1}{2}\int_V d\mathbf{r} \left(\int_{\Omega_+} d\omega \sum_\lambda \tilde{\mathbf{p}}^\dagger_{\omega,\lambda} d^*_{\omega,\lambda} e^{i\omega t} \right) \\ &\cdot \overline{\mathbf{M}} \cdot \left(\int_{\Omega_+} d\omega' \sum_{\lambda'} \tilde{\mathbf{p}}_{\omega',\lambda'} d_{\omega',\lambda'} e^{-i\omega' t} \right) \\ = &\frac{1}{2}\int_{\Omega_+} d\omega \sum_\lambda \int_{\Omega_+} d\omega' \sum_{\lambda'} d^*_{\omega,\lambda} d_{\omega',\lambda'} e^{i(\omega-\omega')t} \\ &\times \left(\int_V d\mathbf{r} \tilde{\mathbf{q}}^\dagger_{\omega,\lambda} \cdot \overline{\mathbf{K}} \cdot \tilde{\mathbf{q}}_{\omega',\lambda'} \right) \\ &+ \frac{1}{2}\int_{\Omega_+} d\omega \sum_\lambda \int_{\Omega_+} d\omega' \sum_{\lambda'} d^*_{\omega,\lambda} d_{\omega',\lambda'} e^{i(\omega-\omega')t} \end{aligned}$$

$$\times \left(\int_V d\mathbf{r} \tilde{\mathbf{p}}^{\dagger}_{\omega,\lambda} \cdot \overline{\mathbf{M}} \cdot \tilde{\mathbf{p}}_{\omega',\lambda'} \right). \tag{D2}$$

Using the relation in the first row equation of (15), a time-harmonic eigenmode for $\mathbf{p}$ can be represented by

$$\tilde{\mathbf{p}}_{\omega,\lambda} = -i\omega \overline{\mathbf{M}}^{-1} \cdot \tilde{\mathbf{q}}_{\omega,\lambda}, \tag{D3}$$

therefore, one can have the following property:

$$\begin{aligned} &\int_V d\mathbf{r} \tilde{\mathbf{p}}^{\dagger}_{\omega,\lambda} \cdot \overline{\mathbf{M}} \cdot \tilde{\mathbf{p}}_{\omega',\lambda'} \\ &= \omega\omega' \int_V d\mathbf{r} (\overline{\mathbf{M}}^{-1} \cdot \tilde{\mathbf{q}}_{\omega,\lambda})^{\dagger} \cdot \overline{\mathbf{M}} \cdot (\overline{\mathbf{M}}^{-1} \cdot \tilde{\mathbf{q}}_{\omega',\lambda'}) \\ &= \omega\omega' \int_V d\mathbf{r} \tilde{\mathbf{q}}^{\dagger}_{\omega,\lambda} \cdot \overline{\mathbf{M}}^{-1} \cdot \tilde{\mathbf{q}}_{\omega',\lambda'} = \omega\omega' \delta_{\omega,\omega'} \delta_{\lambda,\lambda'}. \end{aligned} \tag{D4}$$

Finally, by applying (20) and (D4) to (D2), one can obtain the diagonalized Hamiltonian such as

$$H = \frac{1}{2} \int_{\Omega_+} d\omega \sum_{\lambda} \omega^2 (d^*_{\omega,\lambda} d_{\omega,\lambda} + d_{\omega,\lambda} d^*_{\omega,\lambda}). \tag{D5}$$

APPENDIX E: CROSS-COUPLING DESCRIPTION

Motivated by the recent work to rigorously find time-harmonic eigenmodes for photonic crystal systems by solving an explicit EVP [35], we can derive another GH-EVP, called the *cross-coupling description*. To convert (B2) into a GH-EVP, as performed in Ref. [35], we multiply $\overline{\mathbf{U}}$ to the both sides of (B2) to obtain

$$\omega \overline{\mathbf{U}} \cdot \begin{bmatrix} \tilde{\mathbf{q}}_{\omega,\lambda} \\ \tilde{\mathbf{p}}_{\omega,\lambda} \end{bmatrix} = i\overline{\mathbf{V}} \cdot \begin{bmatrix} \tilde{\mathbf{q}}_{\omega,\lambda} \\ \tilde{\mathbf{p}}_{\omega,\lambda} \end{bmatrix}, \tag{E1}$$

where $i\overline{\mathbf{V}} = \overline{\mathbf{U}} \cdot i\overline{\mathbf{J}} \cdot \overline{\mathbf{U}}$ is now a Hermitian matrix. Finally, solving (E1) yields a complete set of time-harmonic eigenmodes with real eigenfrequencies ω. Furthermore, the following two orthonormal properties can be deduced

$$\int_V d\mathbf{r} \left(\begin{bmatrix} \tilde{\mathbf{q}}_{\omega,\lambda} \\ \tilde{\mathbf{p}}_{\omega,\lambda} \end{bmatrix}^{\dagger} \cdot \overline{\mathbf{U}} \cdot \begin{bmatrix} \tilde{\mathbf{q}}_{\omega',\lambda'} \\ \tilde{\mathbf{p}}_{\omega',\lambda'} \end{bmatrix} \right) = \delta_{\omega,\omega'} \delta_{\lambda,\lambda'}, \tag{E2}$$

$$\int_V d\mathbf{r} \left(\begin{bmatrix} \tilde{\mathbf{q}}_{\omega,\lambda} \\ \tilde{\mathbf{p}}_{\omega,\lambda} \end{bmatrix}^{\dagger} \cdot i\overline{\mathbf{V}} \cdot \begin{bmatrix} \tilde{\mathbf{q}}_{\omega',\lambda'} \\ \tilde{\mathbf{p}}_{\omega',\lambda'} \end{bmatrix} \right) = \omega \delta_{\omega,\omega'} \delta_{\lambda,\lambda'}. \tag{E3}$$

Substituting (B1) into the original Hamiltonian (8) and applying the orthonormal condition (E3), one can easily diagonalize the Hamiltonian in terms of $c_{\omega,\lambda}$ as

$$H = \frac{1}{2} \int_{\Omega_+} d\omega \sum_{\lambda} (c^*_{\omega,\lambda} c_{\omega,\lambda} + c_{\omega,\lambda} c^*_{\omega,\lambda}), \tag{E4}$$

where Ω_+ denotes the positive-frequency regime of Ω.

The manipulation done to derive (E1) is more than a coincidence. In fact, (E1) is closely associated with the energy continuity equation. To check this, let us multiply both sides of (10) by $\overline{\mathbf{U}}$ as follows:

$$\overline{\mathbf{U}} \cdot \left(\frac{\partial}{\partial t} \begin{bmatrix} \mathbf{q} \\ \mathbf{p} \end{bmatrix} \right) = \overline{\mathbf{V}} \cdot \begin{bmatrix} \mathbf{q} \\ \mathbf{p} \end{bmatrix}, \tag{E5}$$

which is the time-domain description of (E1). It should be mentioned that $\overline{\mathbf{U}}$ and $\overline{\mathbf{V}}$ are real matrices and independent of time or frequency. Then multiplying both sides of (E5) by $[\mathbf{q},\ \mathbf{p}]^*$, one arrives at

$$\begin{bmatrix} \mathbf{q} \\ \mathbf{p} \end{bmatrix}^{\dagger} \cdot \overline{\mathbf{U}} \cdot \left(\frac{\partial}{\partial t} \begin{bmatrix} \mathbf{q} \\ \mathbf{p} \end{bmatrix} \right) = \begin{bmatrix} \mathbf{q} \\ \mathbf{p} \end{bmatrix}^{\dagger} \cdot \overline{\mathbf{V}} \cdot \begin{bmatrix} \mathbf{q} \\ \mathbf{p} \end{bmatrix}. \tag{E6}$$

The LHS in (E6) represents an energy density rate over an infinitesimal volume since

$$\begin{aligned} \begin{bmatrix} \mathbf{q} \\ \mathbf{p} \end{bmatrix}^{\dagger} \cdot \overline{\mathbf{U}} \cdot \left(\frac{\partial}{\partial t} \begin{bmatrix} \mathbf{q} \\ \mathbf{p} \end{bmatrix} \right) &= 2\frac{\partial}{\partial t}\mathcal{H} - \left(\frac{\partial}{\partial t} \begin{bmatrix} \mathbf{q} \\ \mathbf{p} \end{bmatrix} \right)^{\dagger} \cdot \overline{\mathbf{U}} \cdot \begin{bmatrix} \mathbf{q} \\ \mathbf{p} \end{bmatrix} \\ &= \frac{\partial}{\partial t}\mathcal{H}, \end{aligned} \tag{E7}$$

where

$$\mathcal{H} = \frac{1}{2} \begin{bmatrix} \mathbf{q} \\ \mathbf{p} \end{bmatrix}^{\dagger} \cdot \overline{\mathbf{U}} \cdot \begin{bmatrix} \mathbf{q} \\ \mathbf{p} \end{bmatrix}. \tag{E8}$$

The energy continuity equation states that an energy density rate should be equal to a negative of an energy flux, viz.,

$$\frac{\partial}{\partial t}\mathcal{H} + \text{energy flux} = 0. \tag{E9}$$

Thus, the RHS in (E6) can be interpreted as a negative of an energy flux flowing out of a closed surface of the infinitesimal volume

$$\text{energy flux} = -\begin{bmatrix} \mathbf{q} \\ \mathbf{p} \end{bmatrix}^{\dagger} \cdot \overline{\mathbf{V}} \cdot \begin{bmatrix} \mathbf{q} \\ \mathbf{p} \end{bmatrix}. \tag{E10}$$

One can easily check that the above energy flux only contains EM-associated terms ($\mathbf{A}$, Φ, $\mathbf{\Pi}_{AP}$, and Π_{Φ}) while $\mathbf{P}$ and $\mathbf{\Pi}_P$ terms are canceled out. This coincides with the explanation in Ref. [36] that Lorentz oscillators do not propagate energy. Furthermore, when polarization density goes to zero, the energy continuity Eq. (E6) converges to the conventional Poynting theorem.

We have shown two possible approaches to derive GH-EVPs for EM fields coupled to lossless Lorentz oscillators and search for a complete set of time-harmonic eigenmodes of the system. The overview is illustrated in Fig. 7.

APPENDIX F: DETAILS OF SIMULATIONS OF THE HONG-OU-MANDEL EFFECT IN A DISPERSIVE BEAM SPLITTER

1. Design of dispersive beam splitter

A dispersionless beam splitter is designed first. Performing a parametric study, we set the relative permittivity of the slab $\epsilon_{s,\infty} = 7\epsilon_0$ [F/m] and the thickness $L_s = 6$ [mm]. The relevant parameters are listed in Table I. It can be observed in Fig. 8 that the 50 : 50 reflectivity $|\mathcal{R}|^2$ and transmissivity $|\mathcal{T}|^2$ with a quadrature phase shift can be achieved around $\omega/c \approx 526$. This frequency $\omega/c \approx 526$ will be used for the

TABLE I. Simulation parameters.

L	1.5 [m]	$N^{(0)}$	2500	x_g	0.3747 [m]
L_s	6 [mm]	Δx	0.6 [mm]	σ_g	0.05 [m]
$\epsilon_{s,\infty}$	7	$N^{(0)}_s$	10	ω_g	$526c$ [rad/s]

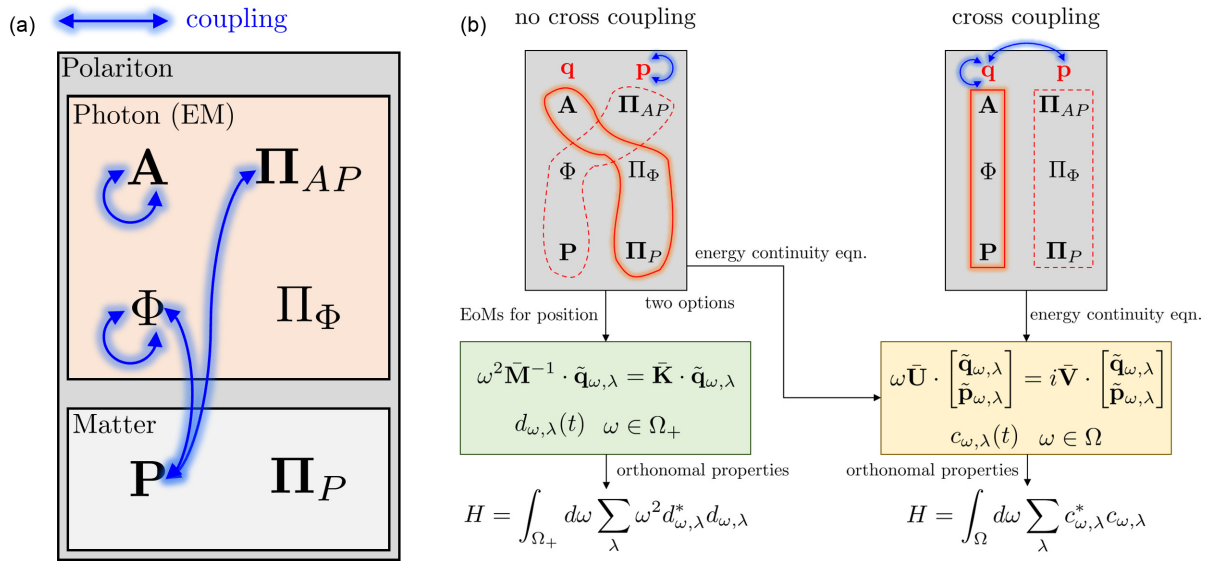

FIG. 7. Overview of the two possible ways to derive GH-EVPs for a coupled system between EM fields and lossless Lorentz oscillators. The schematic in panel (a) describes an overall coupling relation among all dynamical variables in the original Hamiltonian (5). Note that blue solid-glowed line symbolizes coupling between two variables. In panel (b), the left and right schematics depict the no-cross-coupling and cross-coupling descriptions, respectively. In the presence of cross coupling, one should invoke the energy continuity equation to obtain a GH-EVP which yields a full set of time-harmonic eigenmodes for both **q** and **p** with positive and negative eigenfrequencies. In contrast, by properly defining **q** and **p** for no cross coupling, one can either arrive at another GH-EVP in terms of **q** only. Consequently, it yields the smaller eigenspace spanned by time-harmonic eigenmodes for **q** with positive eigenfrequency. Both methods can easily diagonalize the Hamiltonian in terms of modal amplitudes either $c_{\omega,\lambda}$ or $d_{\omega,\lambda}$ via the orthonormal properties inherent from GH-EVPs.

carrier frequency ω_g of incident photons' wave packets. It is to be noted that, even though material dispersion is ignored, geometrical dispersion is present due to the finite thickness of the beam splitter.

The dispersive dielectric slab is modeled by single species Lorentz oscillators. All Lorentz oscillators have same ω_p and ω_0 where $\omega_0^2 = \omega_p^2/(\epsilon_{s,\infty} - 1) + \omega_g^2$. Since the resulting relative dielectric constant becomes $\epsilon_s(\omega) = 1 + \omega_p^2/(\omega_0^2 - \omega^2)$, it always ensures $\epsilon_s(\omega_g) = \epsilon_{s,\infty}$. Figure 9 illustrates the dielectric constant versus ω for various ω_p. Because $\epsilon_s(\omega)$ starts deviating from $\epsilon_{s,\infty} = 7\epsilon_0$ when $|\omega - w_g|$ increases, the bandwidth of exhibiting the 50 : 50 performance becomes narrower. The smaller ω_p (higher dispersion) is, the narrower is the 50 : 50 performance bandwidth.

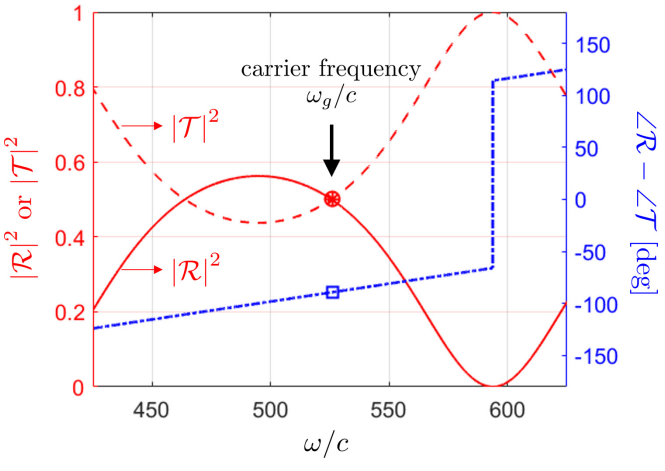

FIG. 8. Reflectivity (solid red line), transmissivity (dashed red line), and their phase difference (dash-dotted blue line) versus ω for the designed dispersionless beam splitter. The 50 : 50 reflectivity and transmissivity with a quadrature phase shift can be achieved around $\omega/c \approx 526$ which will be chosen for the center frequency of incident photons' wave packets.

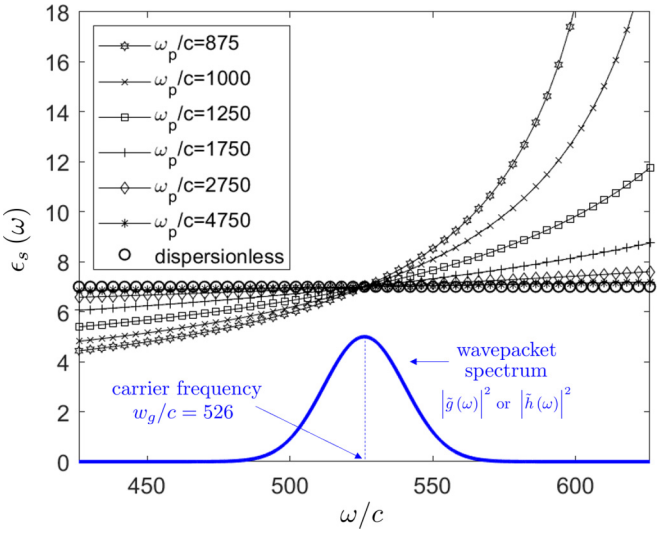

FIG. 9. Relative dielectric constant $\epsilon_s(\omega)$ versus ω for various plasma frequencies. In dispersive cases, since $\epsilon_s(\omega)$ starts deviating from $\epsilon_{s,\infty} = 7\epsilon_0$ as $|\omega - 526c|$ increases, the 50 : 50 performance bandwidth decreases. The smaller ω_p (higher dispersion) is, the smaller the bandwidth becomes.

2. Extraction of numerical eigenmodes

To extract numerical time-harmonic eigenmodes, we use the finite-difference method (FDM) and Bloch-Floquet boundary conditions to numerically solve (30). The problem domain $V \in \{x \in [-L/2, L/2]\}$ is uniformly discretized (grid spacing Δx) by a number $N^{(0)}$ of grid points. The number of grid points inside the beam splitter is $N_s^{(0)}$. Thus, we have total $N^{(0)} + N_s^{(0)}$ numerical time-harmonic eigenmodes having positive eigenfrequencies.

3. Modeling incoming polychromatic photons

Two photons are assumed to be polychromatic, viz., they are riding on wave packets whose spatial distributions are modeled by $g(x)$ and $h(x)$, respectively. The corresponding initial quantum state can be modeled by

$$\begin{aligned}|\Psi^{(2)}\rangle &= \left(\int_{\Omega_+} d\omega \sum_{\lambda} \tilde{g}(\omega,\lambda)\hat{d}^{\dagger}_{\omega,\lambda}\right) \\ &\quad\times \left(\int_{\Omega_+} d\omega' \sum_{\lambda'} \tilde{h}(\omega',\lambda')\hat{d}^{\dagger}_{\omega',\lambda'}\right)|0\rangle \\ &\approx \left(\sum_m \tilde{g}_m \hat{d}^{\dagger}_m\right)\left(\sum_n \tilde{h}_n \hat{d}^{\dagger}_n\right)|0\rangle \\ &= (\tilde{\mathbf{g}}^T\cdot\hat{\mathbf{c}})(\tilde{\mathbf{h}}^T\cdot\hat{\mathbf{c}})\,|0\rangle\,, \end{aligned} \tag{F1}$$

where the second equality is the discrete counterpart of the first one, m and n are numerical time-harmonic eigenmode indices, and $[\tilde{\mathbf{g}}]_m = \tilde{g}_m$ and $[\tilde{\mathbf{h}}]_n = \tilde{h}_n$ are spectral probability amplitudes. If wave packet is modeled by Gaussian function,

$$g(x) = g_0 e^{-(\frac{x-(x_g-\delta x_g)}{\sqrt{2}\sigma_g})^2} e^{-ik_g x}, \tag{F2}$$

$$h(x) = h_0 e^{-(\frac{x+x_g}{\sqrt{2}\sigma_g})^2} e^{ik_g x}, \tag{F3}$$

where the carrier wave number $k_g = \omega_g/c$ and g_0 and h_0 are normalization constants. By using the orthonormal properties of numerical time-harmonic eigenmodes, one can obtain $\tilde{\mathbf{g}}$ and $\tilde{\mathbf{h}}$.

4. Calculation of second-order correlation

We can evaluate the second-order correlation [7,37]

$$g^{(2)}(\tau) = \frac{\langle\Psi^{(2)}|\hat{\alpha}^{(+)}\hat{\beta}^{(-)}\hat{\beta}^{(+)}\hat{\alpha}^{(+)}|\Psi^{(2)}\rangle}{\langle\Psi^{(2)}|\hat{\alpha}^{(-)}\hat{\alpha}^{(+)}|\Psi^{(2)}\rangle\langle\Psi^{(2)}|\hat{\beta}^{(-)}\hat{\beta}^{(+)}|\Psi^{(2)}\rangle}, \tag{F4}$$

where $\tau = \delta x_g/c$ and

$$\hat{\alpha}^{(\pm)} = \hat{A}^{(\pm)}(x_1, t_1), \tag{F5}$$

$$\hat{\beta}^{(\pm)} = \hat{A}^{\pm}(x_2, t_1 + \tau), \tag{F6}$$

$t_1 = 2x_g/c$. The detailed calculation for $g^{(2)}(\tau)$ is explained in Ref. [3].

APPENDIX G: DETAILS OF SIMULATIONS ON NONLOCAL DISPERSION CANCELLATION FOR AN ENERGY-TIME ENTANGLED PHOTON PAIR

1. Modeling energy-time entangled photon pair

Based on a pump frequency $\Omega_P/c = 35$, the signal and idler photons have the center frequencies $\Omega_S/c = 37.5$ and $\Omega_I/c = 32.5$ with a bandwidth of $5c$. The corresponding initial quantum state can be written by

$$\begin{aligned}|\Psi\rangle &= \int_{-\infty}^{\infty} d\omega_2 \sum_{\lambda_2} \int_{-\infty}^{\infty} d\omega_1 \sum_{\lambda_1} \psi(\omega_2,\lambda_2,\omega_1,\lambda_1) \\ &\quad\times \hat{d}^{\dagger}_{\omega_2,\lambda_2}\hat{d}^{\dagger}_{\omega_1,\lambda_1}|0\rangle\,, \end{aligned} \tag{G1}$$

where ψ is a nonfactorizable joint spectral probability amplitude. On the other hand, one can describe a (spatially localized) nonentangled photon pair by

$$\begin{aligned}|\Phi\rangle &= \int_{-\infty}^{\infty} d\omega_2 \sum_{\lambda_2} \int_{-\infty}^{\infty} d\omega_1 \sum_{\lambda_1} \phi_2(\omega_2,\lambda_2)\phi_1(\omega_1,\lambda_1) \\ &\quad\times \hat{d}_{\omega_2,\lambda_2}\hat{d}_{\omega_1,\lambda_1}|0\rangle\,, \end{aligned} \tag{G2}$$

where ϕ_i describes a spectral probability amplitude of ith photon for $i = 1, 2$. By implicitly accounting for the degeneracy index, Figs. 10(a) and 10(b) illustrate $\psi(\omega_2,\omega_1)$ and $\phi(\omega_2,\omega_1) = \phi_2(\omega_2)\phi_1(\omega_1)$.

2. Design of dispersive media

To induce nonlocal dispersion cancellation, we introduce a dispersive medium composed of uniformly filled single species of Lorentz oscillators. And we exploit highly dispersive two local regimes in the dispersion diagram: One is below the band gap for idler photons the other is above the band gap for the signal photons, as illustrated in Fig. 11(a). By properly choosing resonant and plasma frequencies of the media, we can achieve the same magnitude of the second-order dispersion (β) with opposite signs over the photon's bandwidth, as illustrated in Fig. 11(b). The length of the both dispersive media is L_s.

3. Coincidence

We compute the degree of coincidence for the above two cases at different times t_1 and t_2, as depicted in Figs. 10(c) and 10(d), respectively. One can observe that the entangled photon pair has both strong temporal correlation and frequency anticorrelation obeying

$$\Delta(t_2 - t_1)\Delta(\omega_2 + \omega_1 - \Omega_P) \leqslant 1, \tag{G3}$$

where t_2 and t_1 are detection times of the signal and idler photons, respectively. However, the nonentangled photon pair does not exhibit any (anti)correlations.

APPENDIX H: CONSISTENCY WITH PAST WORKS

We show that the present method is consistent with some previous works in some limiting cases.

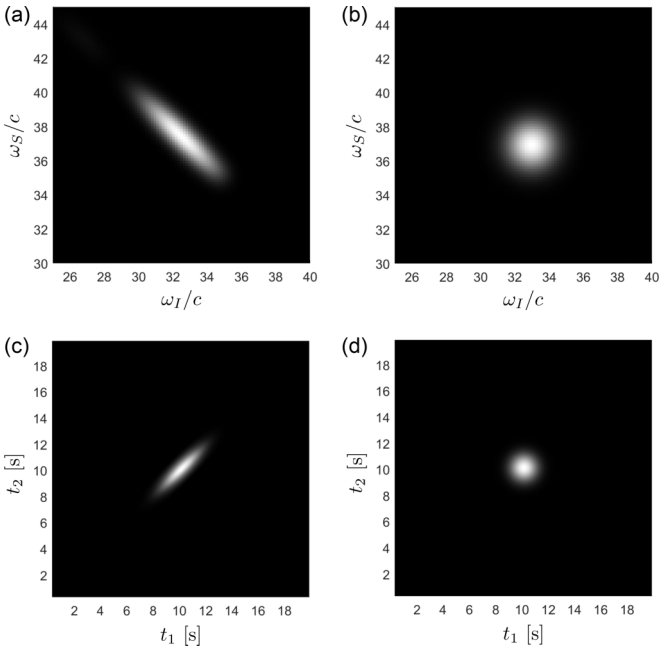

FIG. 10. Spectral probability amplitudes for (a) two entangled photons $\psi(\omega_2, \omega_1)$ and (b) two nonentangled photons $\phi(\omega_2, \omega_1)$. The degree of (two-time) coincidence for (c) entangled and (d) nonentangled photon pairs. The entangled photon pair has both strong temporal correlation and frequency anticorrelation whereas the nonentangled photon pair does not.

1. Free-field quantization

In the vacuum, by using the Coulomb gauge with $\Phi = 0$, there are nonzero dynamical variables $\mathbf{A}$ and $\mathbf{\Pi}_{AP}$. Taking the no-cross-coupling description, one can easily check that (17) is equivalent to the conventional Helmholtz wave equation for $\mathbf{A}$

$$\nabla^2 \tilde{\mathbf{A}}_{\omega,\lambda}(\mathbf{r}) + \omega^2 \epsilon_0 \mu_0 \tilde{\mathbf{A}}_{\omega,\lambda}(\mathbf{r}) = 0, \tag{H1}$$

where analytic solutions are plane waves. The subsequent quantization can be easily done with the plane-wave basis. Note that the plane waves have a dispersion relation $\omega^2 \epsilon_0 \mu_0 = k^2 = |\mathbf{k}|^2$ exhibiting the one-to-one correspondence between ω and $\mathbf{k}$. Thus, a photon has both definite energy and momentum.

2. Inhomogeneous dispersionless dielectric medium

The present methods are still valid when the background vacuum is replaced by a dispersionless inhomogeneous medium, modeled by $\epsilon_\infty(\mathbf{r})$ and $\mu_\infty(\mathbf{r})$, making the resulting EVP still Hermitian. Although this assumption does not satisfy the Kramers-Kronig relation over all frequencies, it will be computationally efficient when dealing with a medium which is almost dispersionless over a narrow bandwidth.

Assume that Lorentz oscillators are absent (viz. no dispersive medium) and the background is filled by dispersionless and inhomogeneous dielectric medium. Using the generalized Coulomb gauge with $\Phi = 0$ and again taking the no coupling approach, one can show that (17) is equivalent to the conventional Helmholtz wave for dispersionless inhomogeneous

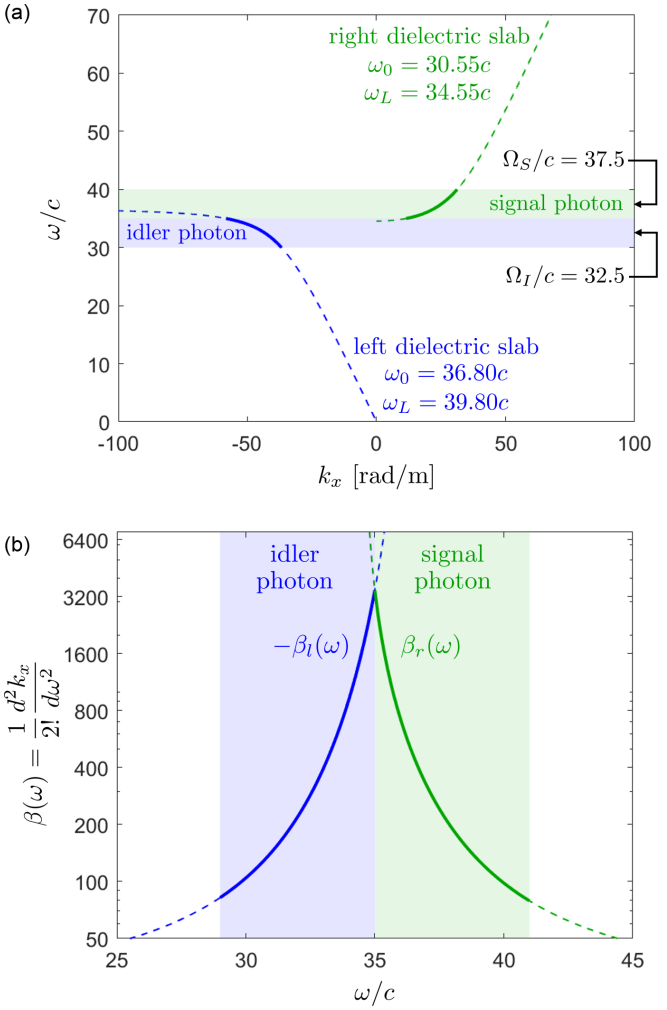

FIG. 11. (a) Dispersion diagram and (b) second-order dispersion β of designed dispersive media. The signal (green lines on the right) and idler (blue lines on the left) photons will experience the almost same amount of second-order dispersions with opposite sign.

dielectric media; viz.,

$$\nabla^2 \tilde{\mathbf{A}}_{\omega,\lambda}(\mathbf{r}) + \omega^2 \epsilon_\infty(\mathbf{r}) \mu_0 \tilde{\mathbf{A}}_{\omega,\lambda}(\mathbf{r}) = 0. \tag{H2}$$

In this case, time-harmonic eigenmodes, which corresponds to Bloch-Floquet modes, do not hold the one-to-one correspondence between ω and $\mathbf{k}$; hence, monochromatic photons cannot have a definite momentum. Canonical quantization can be done with the Bloch-Floquet modes [1–3].

3. One-dimensional homogeneous dispersive medium

A quantized vector potential field operator in 1-D vacuum uniformly filled by lossless Lorentz oscillators, which models a dispersive and homogeneous dielectric medium, was represented by [36,38]

$$\hat{A}(x,t) = \int_{\Omega_+} d\omega \sum_{\lambda=-}^{+} (\mathcal{A}_0 e^{ik_x x} \hat{c}_{\omega,\lambda} e^{-i\omega t} + \text{H.c.}), \tag{H3}$$

$$\hat{\Pi}_{AP}(x,t) = \int_{\Omega_+} d\omega \sum_{\lambda=-}^{+} (\mathcal{D}_0 e^{ik_x x} \hat{c}_{\omega,\lambda} e^{-i\omega t} + \text{H.c.}), \tag{H4}$$

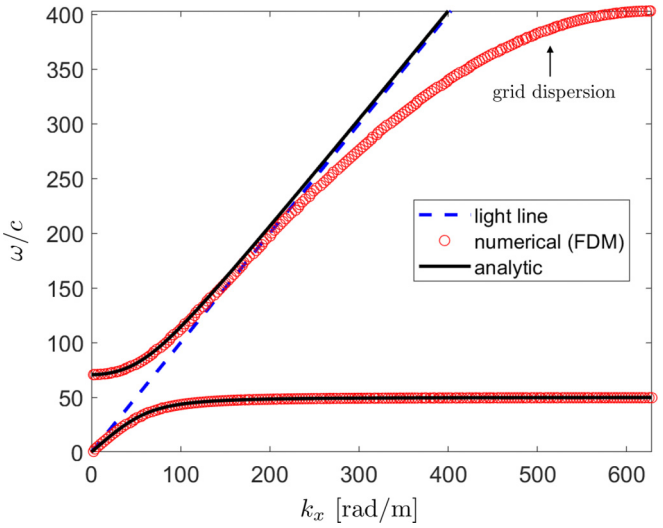

FIG. 12. Dispersion relation (ω, k_x) for a dispersive and homogeneous dielectric medium ($\omega_0 = \omega_p = 50c$). Analytic (blue dashed line) and numerical (red circle) results are compared, showing great agreement except in the high-frequency regime. This is due to the numerical dispersion effect which makes the phase and group velocities gradually slower [39].

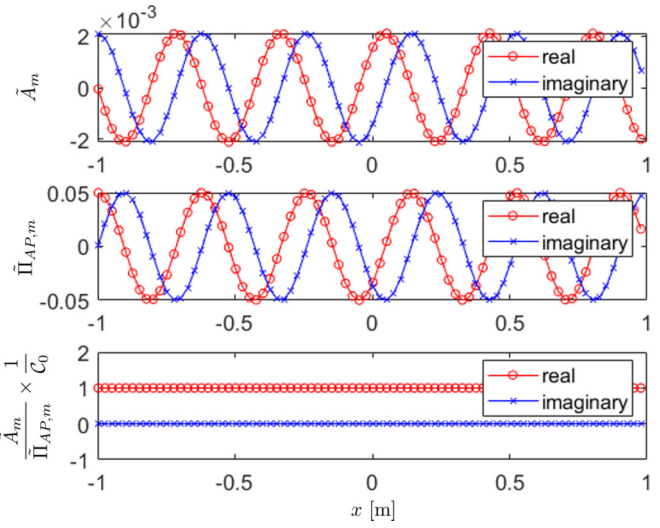

FIG. 13. Illustration of $n = 11$th numerical time-harmonic eigenmode for (a) vector potential and (b) its conjugate variable where $\omega_n \approx 11.52c$. Note that curves with red circles and blue crosses represent real and imaginary values, respectively. The ratio $\tilde{A}_m/\tilde{\Pi}_{AP,m}$ normalized by $\mathcal{C}_0 = i/[\omega\epsilon(\omega_m)]$ is displayed in panel (c), showing that the real and imaginary values are unity and zero, respectively.

where $\lambda = \pm$ denotes the propagation direction degeneracy and

$$\mathcal{A}_0 = -i\sqrt{\frac{\hbar v_g(\omega)}{4\pi\epsilon_0 c\sqrt{\epsilon(\omega)}\omega}}, \tag{H5}$$

$$\mathcal{D}_0 = -\sqrt{\frac{\hbar v_g(\omega)\sqrt{\epsilon(\omega)}^3\omega}{4\pi\epsilon_0 c}}, \tag{H6}$$

where $v_g = d\omega/dk_x$ denotes the group velocity. The dispersion relation is given by $k_x^2 = \omega^2\epsilon(\omega)\mu_0$ where $\epsilon(\omega) = (1 + \frac{\omega_p^2}{\omega_0^2-\omega^2})\epsilon_0$; hence, it also destroys the one-to-one correspondence between ω and k_x. The time-harmonic eigenmodes for $\hat{A}(x,t)$ and $\hat{\Pi}_{AP}(x,t)$ take the form

$$\tilde{A}_{\omega,\lambda}(x) = \mathcal{A}_0 e^{ik_x x}, \tag{H7}$$

$$\tilde{\Pi}_{AP,\omega,\lambda}(x) = \mathcal{D}_0 e^{ik_x x}, \tag{H8}$$

and their ratio becomes

$$\mathcal{C}_0 = \frac{\tilde{A}_{\omega,\lambda}(x)}{\tilde{\Pi}_{AP,\omega,\lambda}(x)} = \frac{\mathcal{A}_0}{\mathcal{D}_0} = \frac{i}{\omega\epsilon(\omega)}. \tag{H9}$$

Taking the cross-coupling description, we use the finite-difference method (FDM), which is widely used across all scientific areas due to its simplicity and reliability, to obtain a set of numerical time-harmonic eigenmodes. The dispersive medium was modeled by Lorentz oscillators (having $\omega_p = \omega_0 = 50c$) uniformly filled over the entire problem domain $x \in [-L/2, L/2]$. Note that the domain was discretized by 201 grid points. Since the present method does not specify wave number of time-harmonic eigenmodes, we performed the spatial fast Fourier transform analysis to extract k_x for each numerical time-harmonic eigenmode. The dispersion relations of analytic and numerical time-harmonic eigenmodes are compared in Fig. 12. There is great agreement between them except in the high-frequency regime. The deviation comes from the numerical grid dispersion error in using the finite-difference approximation [39]. This can be mitigated by using advanced CEM methods, such as finite-element or pseudospectral methods. It is observed that, at a given k_x, there are two plane-wave solutions having different eigenfrequencies lying on the lower and upper branches. The gap between lower and upper branches, i.e., $\omega \in [\omega_0, (\omega_0^2 + \omega_p^2)^{1/2}]$ is related to the anomalous dispersion region if absorption is included [36]. Figure 13 illustrates the $n = 11$th numerical time-harmonic

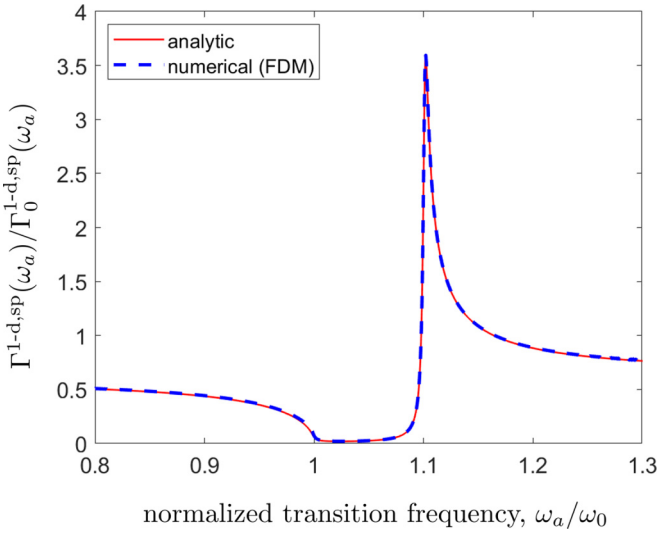

FIG. 14. Purcell factors versus normalized transition frequency ω_a when a two-level system is embedded in a 1-D dispersive medium with a single polarization. The SER can be enhanced above the band gap where $\omega \in [\omega_0, (\omega_0^2 + \omega_p^2)^{1/2}]$.

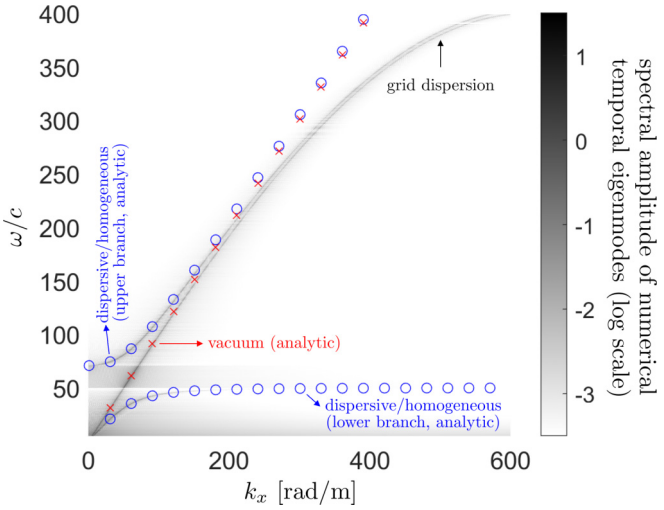

FIG. 15. Dispersion relation (ω, k_x) for the dispersive dielectric slab. The contour map (gray color scale) illustrates spectral amplitudes of numerical time-harmonic eigenmodes. There are three plane-wave solutions having different eigenfrequencies at a given k_x. Two sets of dispersion relations can be observed: One is of the vacuum (red $\times$ marker) and the other is of the dispersive and homogeneous dielectric medium (blue $\circ$ marker).

eigenmodes. One can clearly observe that the ratio between $\tilde{A}_m$ and $\tilde{\Pi}_{AP,m}$ maintains $\mathcal{C}_0$, which is consistent with the analytic time-harmonic eigenmodes.

4. Purcell factor in dispersive medium

Spontaneous emission rate (SER) of an excited atom can be enhanced by introducing cavity [40], plasmonic structures [41], photonic crystals [42], and dielectric media [43]. To check the validity of the proposed method, we compute a Purcell factor when an excited two-level system is embedded in a dispersive medium. For simplicity, we consider the 1-D free space along the x axis and single polarization (electric field operators are polarized along the y axis). The SER of this system can be determined by the Fermi golden rule [44]

$$\Gamma^{\text{1-D,sp}}(\omega_a) = \frac{2\mu_a^2}{3c\hbar^2}\langle 0|\hat{E}_a^{(+)}\hat{E}_a^{(-)}|0\rangle\delta(\omega-\omega_a), \quad \text{(H10)}$$

where ω_a and μ_a denote transition frequency and dipole moment, and

$$\hat{E}_a^{(+)} = \hat{E}^{(+)}(x_a,t) = i\omega\hat{A}^{(+)}(x_a,t) \quad \text{(H11)}$$

at the two-level system's location x_a. We analytically calculate the above SER by using (H3) and approximating $\delta(\omega-\omega_a)$ by Lorentzian distribution. In addition, we evaluate the SER by using numerical time-harmonic eigenmodes based on the no-cross-coupling description. Figure 14 compares Purcell factors versus normalized transition frequency for analytic and numerical time-harmonic eigenmodes. Note that the SER for the 1-D free-space with a single polarization is calculated from the vacuum fields and density of states (DOS) [44]

$$\Gamma_0^{\text{1-D,sp}}(\omega_a) = \frac{\mu_a^2\omega_a}{3\hbar\epsilon_0 c}. \quad \text{(H12)}$$

There is great agreement between two results, which successfully validates the proposed method. The SER can be enhanced above the band gap where $\omega \in [\omega_0, (\omega_0^2+\omega_p^2)^{1/2}]$.

5. One-dimensional dispersive dielectric slab surrounded by free space

Finally, we consider a dispersive dielectric slab (sized by $x \in [-L/4, L/4]$) inside a vacuum box sized by $x \in [-L/2, L/2]$. We take the cross-coupling description to obtain numerical time-harmonic eigenmodes and compute their spectral amplitudes by performing the spatial fast Fourier transform analysis. The result is displayed in Fig. 15, compared with dispersion relations of the vacuum and dispersive and homogeneous dielectric medium. There are three plane-wave solutions with different eigenfrequencies at a given k_x. Two sets of dispersion relations can be observed: One is of the vacuum (red $\times$ marker) and the other is of the dispersive and homogeneous dielectric medium (blue $\circ$ marker). Hence, it is between two limiting cases: (1) vacuum when the slab width converges to zero and (2) dispersive and homogeneous medium when the whole vacuum box is filled by the slab, as expected.

[1] L. Knöll, W. Vogel, and D. G. Welsch, Action of passive, lossless optical systems in quantum optics, Phys. Rev. A **36**, 3803 (1987).
[2] R. J. Glauber and M. Lewenstein, Quantum optics of dielectric media, Phys. Rev. A **43**, 467 (1991).
[3] D.-Y. Na, J. Zhu, W. C. Chew, and F. L. Teixeira, Quantum information preserving computational electromagnetics, Phys. Rev. A **102**, 013711 (2020).
[4] V. Dorier, S. Guérin, and H.-R. Jauslin, Critical review of quantum plasmonic models for finite-size media, Nanophotonics **9**, 3899 (2020).
[5] V. Dorier, J. Lampart, S. Guérin, and H. R. Jauslin, Canonical quantization for quantum plasmonics with finite nanostructures, Phys. Rev. A **100**, 042111 (2019).
[6] J. Poon and B. Francis, Kramers-Kronig relations for lossless media Internal Report (University of Toronto, 2009).
[7] L. Mandel and E. Wolf, *Optical Coherence and Quantum Optics* (Cambridge University Press, Cambridge,1995).
[8] C. Cohen-Tannoudji, J. Dupont-Roc, and G. Grynberg, *Atom-Photon Interactions: Basic Processes and Applications* (Wiley-VCH, New York,1988).
[9] S. Scheel and S. Y. Buhmann, Macroscopic quantum electrodynamics, Acta Phys. Slovaca **58**, 675 (2008).
[10] W. C. Chew, A. Y. Liu, C. Salazar-Lazaro, and W. E. I. Sha, Quantum electromagnetics: A new look-Part I and Part II, IEEE J. Multiscale Multiphysics Comput. Tech. **1**, 73 (2016).
[11] P. A. M. Dirac, *The Principles of Quantum Mechanics* (Clarendon, Oxford, United Kingdom, 1958).

[12] J. M. Jauch and K. M. Watson, Phenomenological quantum-electrodynamics, Phys. Rev. **74**, 950 (1948).

[13] U. Fano, Atomic theory of electromagnetic interactions in dense materials, Phys. Rev. **103**, 1202 (1956).

[14] J. J. Hopfield, Theory of the contribution of excitons to the complex dielectric constant of crystals, Phys. Rev. **112**, 1555 (1958).

[15] J. Plumridge, E. Clarke, R. Murray, and C. Phillips, Ultra-strong coupling effects with quantum metamaterials, Solid State Commun. **146**, 406 (2008).

[16] T. G. Philbin, Casimir effect from macroscopic quantum electrodynamics, New J. Phys. **13**, 063026 (2011).

[17] M. Pelton, Modified spontaneous emission in nanophotonic structures, Nat. Photonics **9**, 427 (2015).

[18] M. S. Tame, K. R. McEnery, Ş. K. Özdemir, J. Lee, S. A. Maier, and M. S. Kim, Quantum plasmonics, Nat. Phys. **9**, 329 (2013).

[19] O. Toader and S. John, Photonic band gap enhancement in frequency-dependent dielectrics, Phys. Rev. E **70**, 046605 (2004).

[20] W. E. I. Sha, A. Y. Liu, and W. C. Chew, Dissipative quantum electromagnetics, IEEE J. Multiscale Multiphysics Comput. Tech. **3**, 198 (2018).

[21] W. C. Chew, *Lectures on Electromagnetic Field Theory* (Purdue University, 2020).

[22] Y. Saad, *Numerical Methods for Large Eigenvalue Problems* (Manchester University Press, Manchester, United Kingdom, 1992).

[23] G. H. Golub and C. F. Van Loan, *Matrix Computations* (Johns Hopkins University Press, Baltimore, 2013).

[24] C. K. Hong, Z. Y. Ou, and L. Mandel, Measurement of Subpicosecond Time Intervals Between Two Photons By Interference, Phys. Rev. Lett. **59**, 2044 (1987).

[25] J. D. Franson, Nonlocal cancellation of dispersion, Phys. Rev. A **45**, 3126 (1992).

[26] H. Fearn and R. Loudon, Quantum theory of the lossless beam splitter, Opt. Commun. **64**, 485 (1987).

[27] S. Prasad, M. O. Scully, and W. Martienssen, A quantum description of the beam splitter, Opt. Commun. **62**, 139 (1987).

[28] C. Gerry and P. Knight, *Introductory Quantum Optics* (Cambridge University Press, Cambridge, 2004).

[29] S.-Y. Baek, Y.-W. Cho, and Y.-H. Kim, Nonlocal dispersion cancellation using entangled photons, Opt. Express **17**, 19241 (2009).

[30] B. Li, F. Hou, R. Quan, R. Dong, L. You, H. Li, X. Xiang, T. Liu, and S. Zhang, Nonlocality test of energy-time entanglement via nonlocal dispersion cancellation with nonlocal detection, Phys. Rev. A **100**, 053803 (2019).

[31] J. Ryu, K. Cho, C.-H. Oh, and H. Kang, All-order dispersion cancellation and energy-time entangled state, Opt. Express **25**, 1360 (2017).

[32] H. Haken, *Quantum Field Theory of Solids: An Introduction* (Elsevier, Amsterdam, The Netherlands, 1983).

[33] T. Lancaster and S. J. Blundell, *Quantum Field Theory for the Gifted Amateur* (Oxford University Press, Oxford, 2014).

[34] C. F. Stevens, *The Six Core Theories of Modern Physics* (MIT Press, Cambridge,, 1995).

[35] A. Raman and S. Fan, Photonic Band Structure of Dispersive Metamaterials Formulated as a Hermitian Eigenvalue Problem, Phys. Rev. Lett. **104**, 087401 (2010).

[36] B. Huttner, J. J. Baumberg, and S. M. Barnett, Canonical quantization of light in a linear dielectric, Europhys. Lett. **16**, 177 (1991).

[37] R. J. Glauber, The quantum theory of optical coherence, Phys. Rev. **130**, 2529 (1963).

[38] K. J. Blow, R. Loudon, S. J. D. Phoenix, and T. J. Shepherd, Continuum fields in quantum optics, Phys. Rev. A **42**, 4102 (1990).

[39] A. Taflove and S. C. Hagness, *Computational Electrodynamics: The Finite-Difference Time-Domain Method*, 3rd ed. (Artech House, Norwood, 2005).

[40] P. Goy, J. M. Raimond, M. Gross, and S. Haroche, Observation of Cavity-Enhanced Single-Atom Spontaneous Emission, Phys. Rev. Lett. **50**, 1903 (1983).

[41] Y. P. Chen, W. E. I. Sha, W. C. H. Choy, L. Jiang, and W. C. Chew, Study on spontaneous emission in complex multilayered plasmonic system via surface integral equation approach with layered medium Green's function, Opt. Express **20**, 20210 (2012).

[42] D. Englund, D. Fattal, E. Waks, G. Solomon, B. Zhang, T. Nakaoka, Y. Arakawa, Y. Yamamoto, and J. Vučković, Controlling the Spontaneous Emission Rate of Single Quantum Dots in a Two-Dimensional Photonic Crystal, Phys. Rev. Lett. **95**, 013904 (2005).

[43] S. M. Barnett, B. Huttner, and R. Loudon, Spontaneous Emission In Absorbing Dielectric Media, Phys. Rev. Lett. **68**, 3698 (1992).

[44] M. Fox, *Quantum Optics: An Introduction* (Oxford University Press, Oxford, 2006), Vol. 15.